Supplementary Information for

Nitrate-to-Ammonia Conversion at Plasmonic Antenna-Reactor Catalyst

Weihui Ou,*[a] Ying Guo,[b,c] Jing Zhong,[b] Fucong Lyu,[b,d,e] Junda Shen,[b] Hongkun Li,[b] Shaoce Zhang,[b] Zebiao Li,[d] Zhijian He,[a] Jun He,[a] Quanxi Mo,[a] Chunyi Zhi,*[b] Yang Yang Li,*[b,e] and Jian Lu*[b,d,e]

Abstract: Electrochemical conversion of nitrate to ammonia is an appealing route to efficiently synthesizing ammonia at ambient conditions while reducing environmental nitrate pollutants. However, this approach is obstructed by the limited yield, selectivity, and faradaic efficiency (FE) of ammonia due to the sluggish multi-electron/proton-involved steps and the competing reaction of hydrogen evolution. Here, we demonstrate a plasmon-assisted strategy to improve the performance of nitrate-to-ammonia electrochemical conversion by constructing plasmonic antenna-reactor catalysts, where Au and Pd nanoparticles/hydrogen substituted graphdiyne (Pd/HsGDY) work as light antenna and reaction site, respectively. Plasmonic excitation of Au-Pd/HsGDY catalysts can remarkably accelerate the nitrate reduction, with the yield rate, selectivity, and FE of ammonia respectively increased by 14.3, 2.1, and 1.8 times under optimal conditions. Mechanistic investigations unveil that Au plasmon-induced hot electrons facilitate nitrate-to-ammonia reaction by regulating the adsorption of reaction intermediates on Pd/HsGDY, wherein the rate-determining step was shifted from nitrate adsorption to the *NH protonation and the overall apparent activation was reduced. Moreover, hot electrons suppress the competing hydrogen evolution by enlarging Gibbs free energy of hydrogen formation. These results open the avenue to develop a desirable catalyst for producing value-added ammonia from environmentally hazardous nitrate by a synergistic combination of electricity and light.

Experimental Procedures

Chemicals

Sodium sulfate (Na_2SO_4, ≥99.0%), Sodium nitrate ($NaNO_3$, ≥99.0%), and ^{15}N potassium nitrate ($Na^{15}NO_3$, ≥99.0%), salicylic acid ($C_7H_6O_3$), trisodium citrate dehydrate ($Na_3C_6H_5O_7 \cdot 2H_2O$), sodium nitroferricyanide ($Na_2[Fe(CN)_5NO] \cdot 2H_2O$, ≥99.0%), sodium hypochlorite solution (NaClO, available chlorine 4.0 wt %), hydrazine monohydrate ($N_2H_4 \cdot H_2O$, ≥99.8%), para(dimethylamino)-benzaldehyde ($C_9H_{11}NO$), deuterated dimethyl sulfoxide (DMSO-d6, 99.9%), chloroform ($CHCl_3$, ≥99.8%), sulfanilamide ($C_6H_8N_2O_2S$, ≥98.0%), and N-(1-naphthyl) ethylenediamine dihydrochloride ($C_{12}H_{16}C_{l2}N_2$ ≥98.0%) were purchased from Sigma-Aldrich (Merck). Concentrated hydrochloric acid (HCl), ammonium sulfate ($(NH_4)_2SO_4$, ≥99.0%), sodium hydroxide (NaOH, ≥96.0%), and sodium nitrite ($NaNO_2$, ≥99.0%) were obtained from Sinopharm Chemical Reagent Co. Ltd. All chemicals were used as received without any further purifications.

Characterization

The morphology and structures were characterized by scanning electron microscopy (SEM, FEI Quanta 200F) and transmission electron microscopy (TEM, jeol tem 2100F FEG operated with an accelerating voltage of 200 kV). X-ray Diffraction (XRD) patterns were collected on an X-ray diffractometer (Rigaku Smartlab) with Cu-Kα radiation (λ = 1.5405 Å). X-ray photoelectron spectroscopy (XPS) conducted on a VG Kα Probe spectrometer (Thermo Fisher Scientific) with Al Kα radiation as the excitation source provide information regarding the oxidation state and bonding environment of Ag, C and Pd with an energy step of 0.1 eV. The absorption spectra were collected using a Shimadzu UV3600 UV-vis-NIR spectrometer. Raman scattering measurements were carried out in backscattering geometry with a Renishaw spectrometer operating at 532 nm laser (Euromex). Fourier Transform infrared spectroscopy (FT-IR) in the range 400-4000 cm^{-1} were recorded on a Thermo Fisher iS50R FT-IR spectrophotometer. Solution ^1H NMR spectra were recorded on a Bruker Avance NEO 400MHz superconducting magnet high-field NMR spectrometer at room temperature. In-situ Raman spectra were collected using a portable Raman spectrometer (ACCUMAN SR-510 Pro, Ocean Optics) with a 785 nm laser.

Preparation of Au-Pd/HsGDY plasmonic antenna-reactor photoelectrocatalyst. The Pd/HsGDY was prepared by a previously developed method. In detail, 30 mg $Pd(OAc)_2$ and 15 mg CuI were ultrasonically dispersed in a mixture solution containing 50 mL of tetrahydrofuran and 50 mL of trimethylamine. After the addition of 200 mg 1,3,5-triethynylbenzene, the mixture solution was heated at 60 °C for 24 h. Then, the resultant solution was centrifuged to discard the supernatant. The yellow precipitate was washed with copious amount of distilled water and ethanol, and then treated with 3 M HNO_3 for 12 h to remove the Cu residue, and finally calcinated at 350°C with a ramp rate of 2^{o}C/min under Ar atmosphere for 2 h to obtain Pd/HsGDY. 10 mg Pd/HsGDY was ultrasonically dispersed in a mixture of distilled water (1 mL) and isopropyl alcohol (1 mL). 20 μL of thus-obtained mixture solution was drop cast on a carbon paper (1 × 1 cm^2) and dried at room temperature, resulting in a loading mass of 0.2 mg/cm^2. This carbon paper was placed in a JEOL smart coater (DII-29030SCTR) for Au deposition using magnetically sputtering method. The sputtering was performed in 6.0 Pa, with the carbon paper positioning 20 mm from Au target source. The sputtering time was 60 s. Thus-obtained Au-Pd/HsGDY on carbon paper was used as plasmonic antenna-reactor photoelectrocatalyst.

Preparation of Pd hydride nanodendrites[1]. 38.5 mg of Pd(acac), 2, 0.1 g of 2-methylimidazole, 250 mg of PVP, and 1 g of ascorbic acid were dissolved in 60 mL of DMF. This mixture was poured into to a Teflon lined reactor and held at 160 °C for 5 h, followed by centrifugation at 9000 rpm for 3 min. The precipitate was washed with ethanol and water to obatin Pd nanodendrites. 10 mg of Pd nanodendrites were dispersed in 20 mL of DMF and heated at 160 °C for 20 h in a Teflon lined reactor. The Pd hydride nanodendrites was obtained by subsequent centrifugation at 9000 rpm 3 min, washed with ethanol and water 3 times and dried at room temperature.

Electrochemical reduction of NO_3^- at Au-Pd/HsGDY photoelectrocatalyst

The Au-Pd/HsGDY deposited on carbon paper was cut into long strips with width of 0.3 cm. One strip was immersed in 45 mL aqueous solution of 0.5 M Na_2SO_4 and 0.1 M $NaNO_3$ as the working electrode in a typical three-electrode system, with its bottom staying 0.5 cm away from the electrolyte surface. The Pt wire and an AgCl/Ag electrode in the saturated KCl solution worked as the counter and reference electrodes, respectively. The electrolyte purged by the Ar gas for 20 min before any conduct. For light experiments, a supercontinuum fibre laser (SuperK FIANIUM FIU-15, 400-2500 nm, 78 MHz, NKT Photonics, Denmark) was used to illuminate the working electrodes, with a short-pass filter with a cut-off wavelength at 900 nm (Thorlabs, United States). The time duration of light illumination was kept same to that of electrochemical reduction of NO_3^- under dark conditions.

For the wavelength-dependent experiments, a bandwidth-tunable filter (SuperK VARIA, NKT Photonics, Denmark) was coupled to the light source (SuperK FIANIUM FIU-15). Seven 50-nm wide bands centered at 425, 525, 625, 725 and 825 nm were selected, and their intensities were set be 7.99 W cm^{-2} by tuning the output power of the light source.

In the intensity-dependent experiment, the illumination light was set at 550 nm with a bandwidth of 100 nm, and the electrode was biased at −0.6 V. The light intensity was controlled by adjusting the output power of the supercontinuum fiber laser and measured to be 0.17, 0.56, 4.31, 9.17, 12.60, and 16.09 W cm^{-2}.

Determination of NH_3 produced during the NO_3^- electrochemical reduction

The amount of produced NH_3 was determined by the indophenol blue method. In detail, the electrochemical reduction of NO_3^- was carried out at investigated electrode potentials in the gas-tight cell (100 mL) containing 45 mL of electrolyte (0.5 M Na_2SO_4+0.1 M $NaNO_3$). After 30 min, 2 mL of electrolyte was collected for determination. In this electrolyte was first added 1.25 mL of aqueous solution containing NaOH (0.625 M), salicylic acid (0.36 M) and sodium citrate (0.17 M). Then, 150 μL of sodium nitroferricyanide solution (10 mg/mL) and 75 μL of NaClO (available chlorine 4.0 wt %) solution was sequentially added. After colorimetric reaction under ambient conditions for 2 h, the UV−vis absorption spectra was recorded from 500 nm to 800 nm using UV−vis Lambda 2S spectrometer. The intensity of peak at 658 nm was used for quantification. The calibration curve was established using the $(NH4)_2SO_4$ solutions within concentration range between 0 μM and 100 μM for the colorimetric reaction under identical conditions. The FE for NH_3 production was calculated following the equation:

$$FE(NH_3) = \frac{8 \times F \times V \times C_{NH_4^+}}{Q}$$

Where, $C_{NH_4^+}$ is the measured concentration of NH_4^+ (mol/L), *F* is the Faraday's constant (96485 C/mol), *V* denotes the volume of electrolyte (0.045 L), and *Q* represents the quantify of charge passed through the electrochemical station.

Determination of NO_2^- during the NO_3^- electrochemical reduction

The amount of produced NO_2^- was determined by the Griess test. Specifically, the electrochemical reduction of NO_3^- proceeded at investigated electrode potentials for 30 min in the gas-tight cell (100 mL) containing 45 mL of electrolyte (0.5 M Na_2SO_4+0.1 M $NaNO_3$). In 5 mL of electrolyte was added 100 μL of aqueous solution containing HCl (2.0 M) and sulfanilamide (10 mg/mL). After 10 min, 100 μL of N-(1-naphthyl) ethylenediamine dihydrochloride (10 mg/mL) was injected. The UV−vis absorption spectra were recorded from 450 nm to 650 nm. The intensity of peak at 538 nm was used for quantification. The calibration curve was established using the $NaNO_2$ solutions within concentration range from 0 μg/mL to 1 μg/mL through the identical procedure. The FE for NO_2^- production was calculated according to the following formula:

$$FE(NO_2^-) = \frac{2\times F\times V\times C_{NO_2^-}}{Q}$$

Where, $C_{NO_2^-}$ is the measured concentration of NO_2^- (mol/L), *F* is the Faraday's constant (96485 C/mol), *V* denotes the volume of electrolyte (0.045 L), and *Q* represents the quantify of charge passed through the electrochemical station.

Measurement of N_2H_4 during the NO_3^- electrochemical reduction

The N_2H_4 was tested by the Watt and Chrisp's method. Specifically, the electrochemical reduction of NO_3^- proceeded at investigated electrode potentials for 30 min in the gas-tight cell (100 mL) containing 45 mL of electrolyte (0.5 M Na_2SO_4+0.1 M $NaNO_3$). In 1 mL of electrolyte was added 1mL of ethanolic solution containing HCl (1.29 M) and para(dimethylamino)-benzaldehyde (17.86 mg/mL). After 30 min, the UV−vis absorption spectra of the reaction solution were recorded from 420 nm to 540 nm. The intensity of peak at 458 nm was used for quantification. We built the calibration curve through the identical colorimetric procedure using the $NaNO_2$ solutions with a series of concentrations.

Detection of H_2 produced during the NO_3^- electrochemical reduction

The electrochemical reduction of NO_3^- was carried out at investigated electrode potentials in the gas-tight cell (100 mL) containing 45 mL of electrolyte (0.5 M Na_2SO_4+0.1 M $NaNO_3$). After 30 min, 100 μL of gas was withdrawn from the headspace of the gas-tight cell using a syringe and injected into gas chromatography (Shimadzu GC-2014) for measurement. The FE for H_2 generation was calculated following the equation:

$$FE(H_2) = \frac{2\times F\times n_{H_2}}{Q}$$

Where, n_{H_2} is the amount of hydrogen (mol), *F* is the Faraday's constant (96485 C/mol), and *Q* represents the quantify of charge passed through the electrochemical station.

Isotope labeling experiments

The isotope-labeled NO_3^- reduction experiments were carried out using the above- mentioned methods, except $NaNO_3$ was replaced with $Na^{15}NO_3$. The *p*H of thus-obtained electrolyte was acidified to be 1-2 with 0.5 M H_2SO_4 solution. Then, 0.6 mL of this acidified electrolyte was mixed with 100 μL of DMSO-d_6, and 2 μL of $CHCl_3$ (internal proton standard). The resultant mixture was subjected to 1H NMR spectroscopy (Bruker Avance NEO 400MHz).

Transient absorption spectroscopy measurement

Femtosecond transient absorption spectra were recorded by a pump−probe spectrometer (Ultrafast, Helios) together with an amplified Ti:sapphire laser source (800 nm with a repetition rate of 1 kHz, Coherent). The ultrafast laser was split into two beams by a beam splitter. One part was sent into an optical parametric amplifier (OPerA Solo, Coherent) to generate pump light whose center wavelength was 500 nm (pulse width <35 fs; output energy ~7 μJ/pulse at the sample cell); the other part was focused on the sapphire crystal to obtain white light continuum (420–820 nm) as probe light to examine the absorption change of samples. The delay between pump light and probe light was tuned by the delay line (minimum step: 50 fs; maximum delay: ~5 ns). The Au/HsGDY and Au-Pd/HsGDY were dispersed into ultrapure water to obtain the homogeneous colloidal solution and subsequently sealed in a transparent cell during measurements, which was mounted on a rotating stage for keeping the pump-excited fraction of sample fresh. All the measurements were under ambient condition.

X-ray absorption spectroscopy measurement

X-ray absorption spectroscopy (XAS) measurements were carried out at performed at the BL08B2 of SPring-8 (8 GeV, 100 mA), Japan. The X-ray beam was mono-chromatized with water-cooled Si (111) double-crystal monochromator and focused with two Rh coated focusing mirrors with the beam size of 2.0 mm in the horizontal direction and 0.5 mm in the vertical direction around sample position, to obtain X-ray adsorption fine structure spectra both in near and extended edge. Au foil, Pd foil and PdO samples were used as references.

Calculation of the utilization of light energy

Assuming the overpotential of anodic electrode (the water oxidation) is zero, the utilization of light energy (η) for NO_3^--to-NH_3 electrochemical conversion at different electrode potentials was calculated using the following equation.

$$\eta = \frac{(1.23\ V - E_{NH_3}^{eq}) \times \Delta Y_{NH_3} \times n \times F}{M_{NH_3} \times P \times 3600} \times 100\%$$

where $E_{NH_3}^{eq}$ is the equilibrium potential (0.70 V) of nitrate electroreduction to ammonia in alkaline media; ΔY_{NH_3} denotes the increment of yield rate of NH_3 induced by light illumination; n is the total charge transfer number (8); *F* is Faradaic number (96500 C/mol); M_{NH_3} is the molar mass of NH_3 (17 g/mol); P represents the intensity of light power (135.1 W/cm^2); the overpotential of anodic electrode (the water oxidation) is assumed zero.

Calculation of the energy consumption of NH_3

We calculated the energy consumption ($E.C.$, kwh/kg) of NH_3 on our catalyst at various electrode potentials following the equation[2]:

$$E.C. = \frac{n \times F \times (1.23\ V - E)}{FE_{NH_3} \times M_{NH_3} \times 3600}$$

where n is the total charge transfer number (8); *F* is Faradaic number (96500 C/mol); FE_{NH_3} represents the Faradaic efficiency of NH_3; M_{NH_3} is the molar mass of NH_3 (17 g/mol); the overpotential of anodic electrode (the water oxidation) is assumed zero; the light energy is assumed free of charge.

Computational details

Theoretical calculations were carried out with plane-wave-based density functional theory (DFT) method in the Vienna Ab Initio Simulation Package (VASP)[3]. The projector augmented wave (PAW) pseudopotentials[4] and Perdew-Burke-Ernzerhof (PBE) functionals[5] were used for VASP. The energy cutoff of plane wave was set at 500 eV. Initially, the Pd(111) surface was built by a 3×3×6 slab with 15 Å of vacuum space. Then, the Pd atoms in bottom one layer were substituted by Au atoms to simulate the conditions in experiment. The new supercell (Pd_5Au) was then optimized, and the lattice parameters were a = 8.327 Å, b = 7.211 Å, c = 26.838 Å, α = β = 90°, γ = 120°. A Monkhorst-Pack grid with size of 3×3×1 was used to sample the Brillouin zone[6]. The optimized geometry was obtained by minimizing the forces on the atoms to below 0.015 eV/Å. A self-consistent field (SCF) convergence with a threshold value of 10^{-7} eV was used for all calculations. VASPKIT code was used for data post-processing and thermodynamic corrections of the gas and adsorbate[7]. The excited-state calculation was performed by promoting one electron from the highest occupied molecular orbitals (HOMO) to the lowest unoccupied molecular orbitals (LUMO) at each k point[8]. The nitrate reduction reaction (NO_3RR) was studied on the $Pd_5Au(111)$ surface. The elementary steps for the reduction of NO_3^- to NH_3 involve the transfer of nine protons and eight electrons. The free energy changes of each elementary steps were simulated by the following equations (* represents the adsorption site)

$$NO_3^- + * \rightarrow *NO_3 + e^-$$

$$*NO_3 + H_2O + 2e^- \rightarrow *NO_2 + 2OH^-$$

$$*NO_2 + H_2O + 2e^- \rightarrow *NO + 2OH^-$$

$$*NO + H_2O + e^- \rightarrow *NHO + OH^-$$

$$*NHO + e^- \rightarrow *N + OH^-$$

$$*N + H_2O + e^- \rightarrow *NH + OH^-$$

$$*NH + H_2O + e^- \rightarrow *NH_2 + OH^-$$

$$*NH_2 + H_2O + e^- \rightarrow *NH_3 + OH^-$$

$$*NH_3 \rightarrow * + NH_3$$

The Gibbs free energies (ΔG) were calculated based on the standard hydrogen electrode model by equation,

$$\Delta G = \Delta E + \Delta E_{\mathrm{ZPT}} - T\Delta S$$

where ΔE, ΔE_{ZPT}, T and ΔS represent the DFT calculated adsorption energy, zero-point energy change, temperature, and entropy differences between the adsorption state and the gas state (298.15 K and 1 atm), respectively. For NO_3^- reduction, the DFT calculated adsorption energy ΔE, $\Delta E_{ZPT} - T\Delta S$ and the Gibbs free energy ΔG of various species in the reaction pathways were listed in **Table S3**. For hydrogen evolution reaction, the ΔE_{ZPT} and ΔS were obtained in the previous study[9], then ΔG_{H^*} was calculated by equation,

$$\Delta G_{H^*} = \Delta E_{H^*} + 0.24\ \mathrm{eV}$$

To avoid directly calculate the energy of charged species, the thermodynamic cycle (**Scheme S1**) was used to determine the adsorption Gibbs free energy of NO_3^-. The adsorption of NO_3^- was described as

$$* + HNO_3(g) \rightarrow *NO_3 + H^+ + e^-$$

So, the adsorption Gibbs free energy of NO_3^- ($\Delta G_{ads}(*NO_3)$) was described as

$$\Delta G_{ads}(*\mathrm{NO_3}) = G(*\mathrm{NO_3}) - G(*) - G\big(\mathrm{HNO_3(g)}\big) + \frac{1}{2}G(H_2(\mathrm{g})) + \Delta G_{correct}$$

$$\Delta G_{correct} = -\Delta G_1 - \Delta G_2$$

where $G(*NO_3)$, $G(*)$, $G(HNO_3(g))$ and $G(H_2(g))$ are the Gibbs free energy of NO_3^- adsorbed on $Pd_5Au(111)$, $Pd_5Au(111)$ substrates, HNO_3 and H_2 molecules in the gas phase, respectively. $\Delta G_{correct}$ denotes the correction of adsorption energy. ΔG_1 and ΔG_2 were given as -0.075 eV and -0.317 eV, respectively[10, 11]. Therefore, $\Delta G_{correct}$ was set at 0.075 + 0.317 = 0.392 eV.

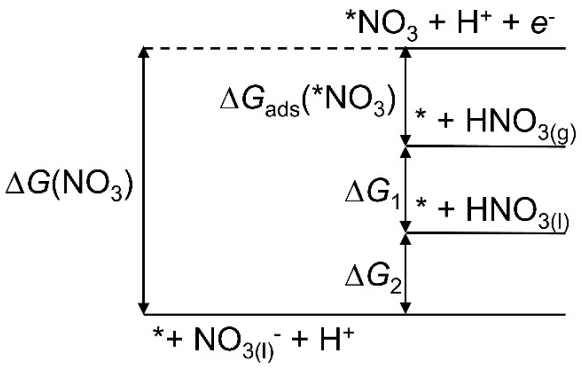

Scheme S1 | Schematic illustration of the thermodynamic cycle used to determine the adsorption Gibbs free energy of NO_3^-[11].

Results and Discussion

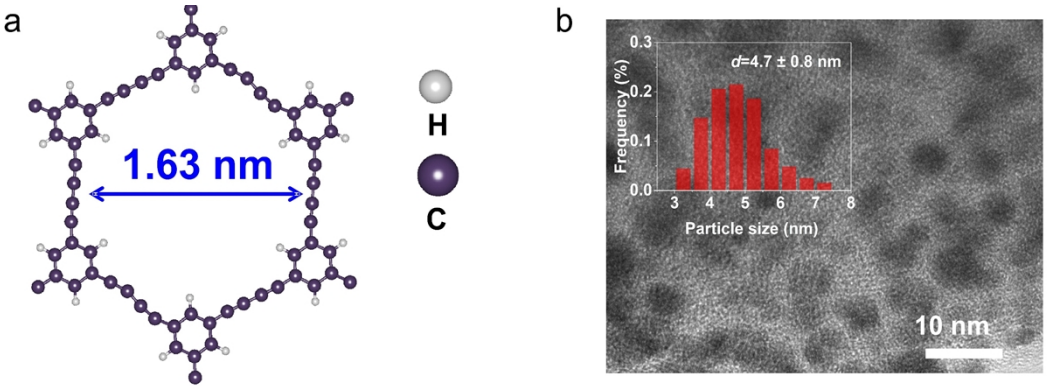

Fig. S1 a) Molecular structure of HsGDY, with the grey white and purple spheres representing H and C atoms, respectively. b) HRTEM image of Pd/HsGDY. The inset is the size distribution of Pd nanoparticles.

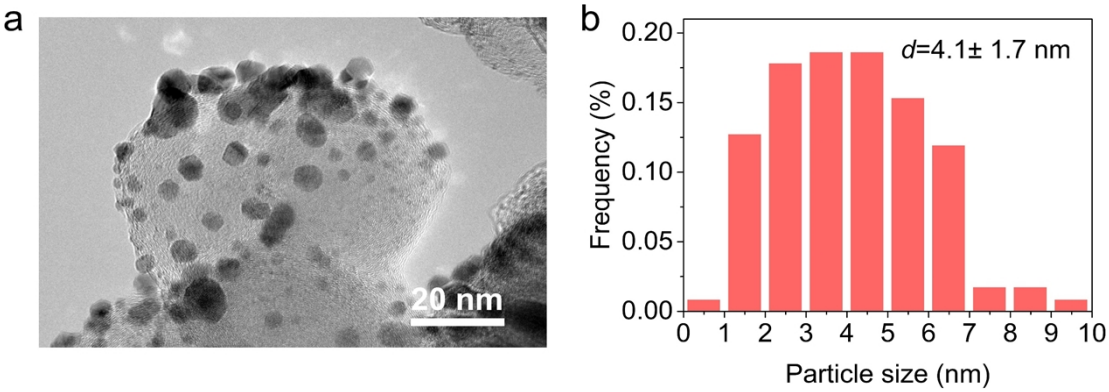

Fig. S2 a) TEM image of Au/HsGDY. b) The size distribution of Au nanocrystals.

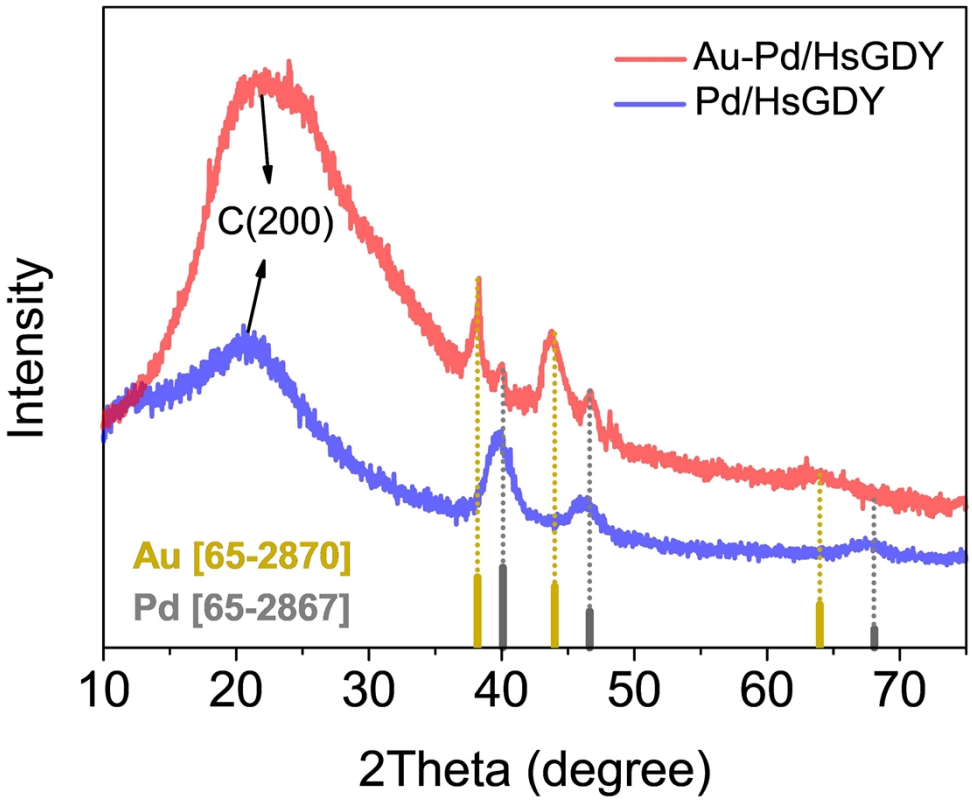

Fig. S3 XRD patterns of Pd/HsGDY and Au- Pd/HsGDY. The dot lines were added for convivence of peaks assignment.

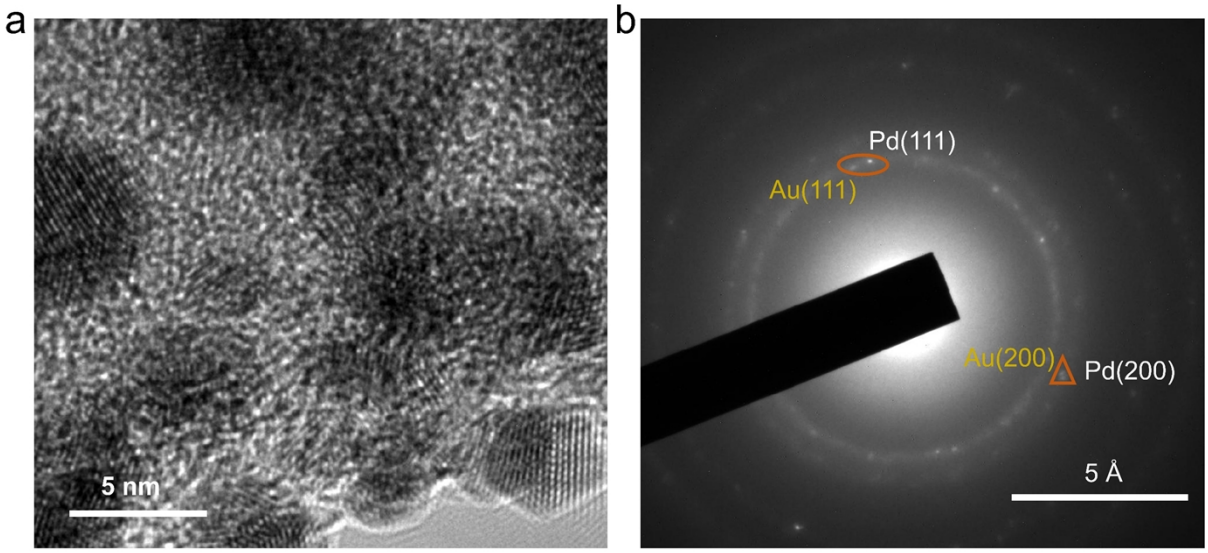

Fig. S4 a) High resolution TEM images of Au-Pd/HsGDY. b) The corresponding selected area electron diffraction patterns.

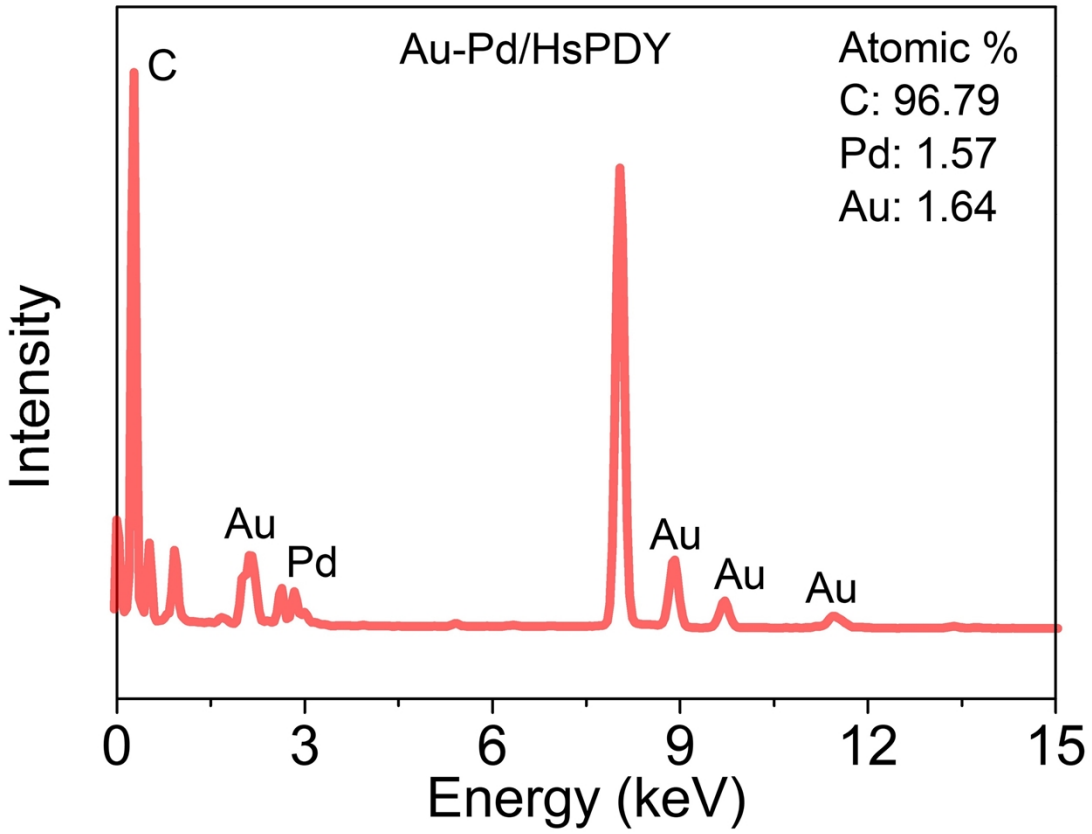

Fig. S5 Energy dispersive spectrum of Au-Pd/HsGDY.

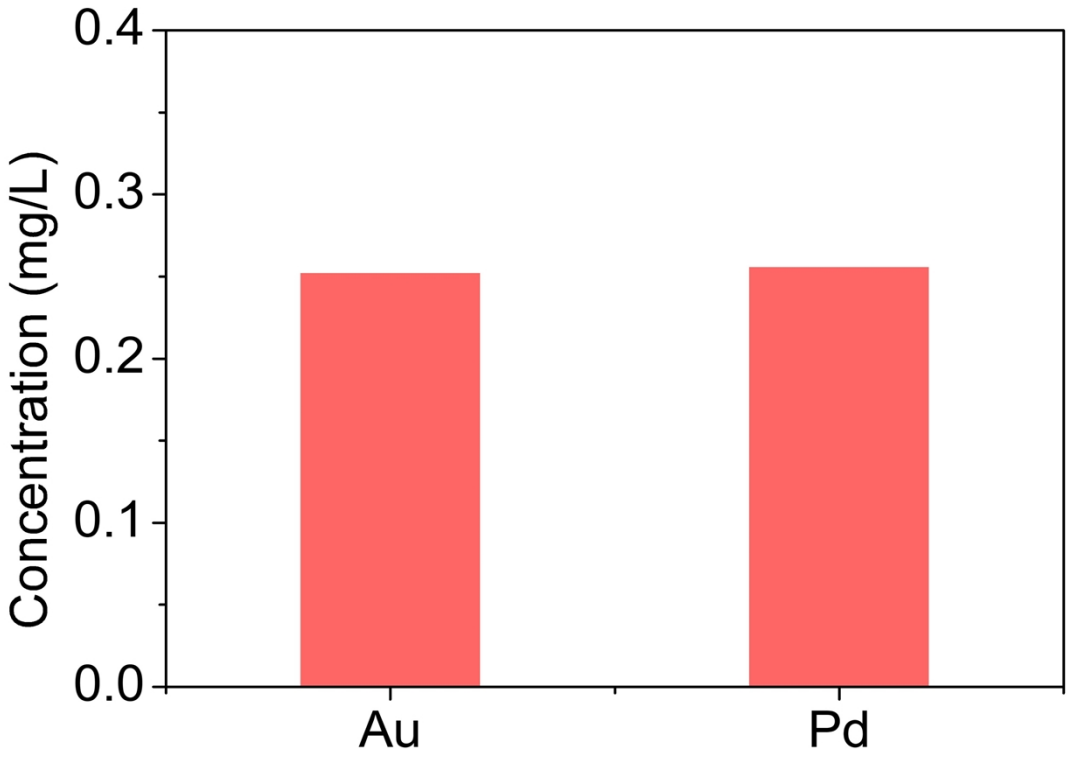

Fig. S6 The concentration of Au and Pd in the digested solution measured by inductively coupled plasma mass spectrometry measurement.

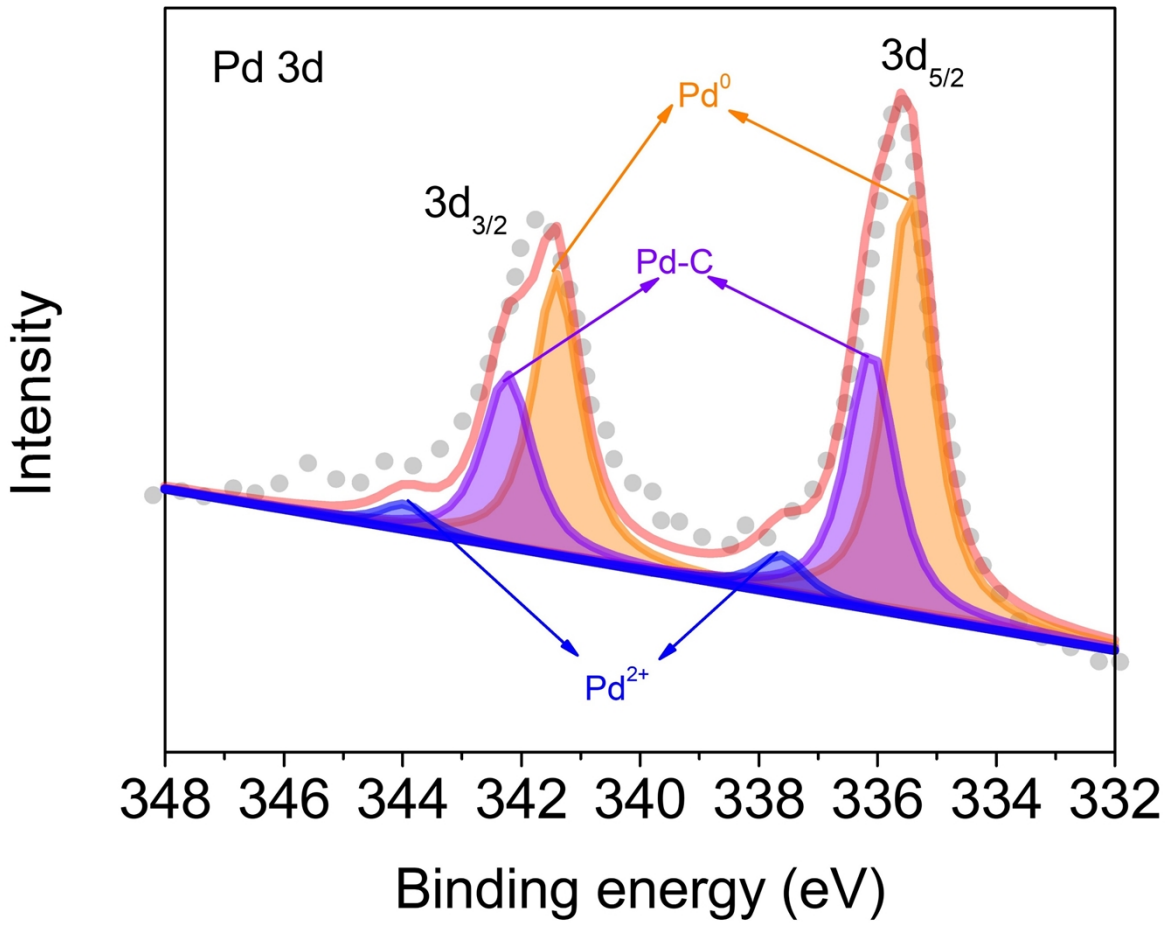

Fig. S7 Pd 3d core-level X-ray photoelectron spectrum (XPS) of Au-Pd/HsGDY.

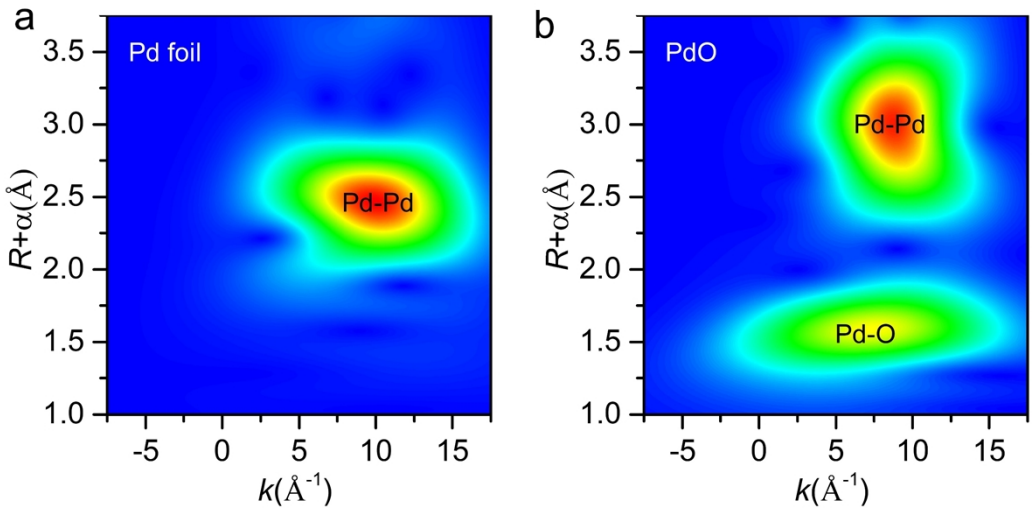

Fig. S8 WT-EXAFS plots of Pd K edge in Pd foil (a) and PdO (b) reference.

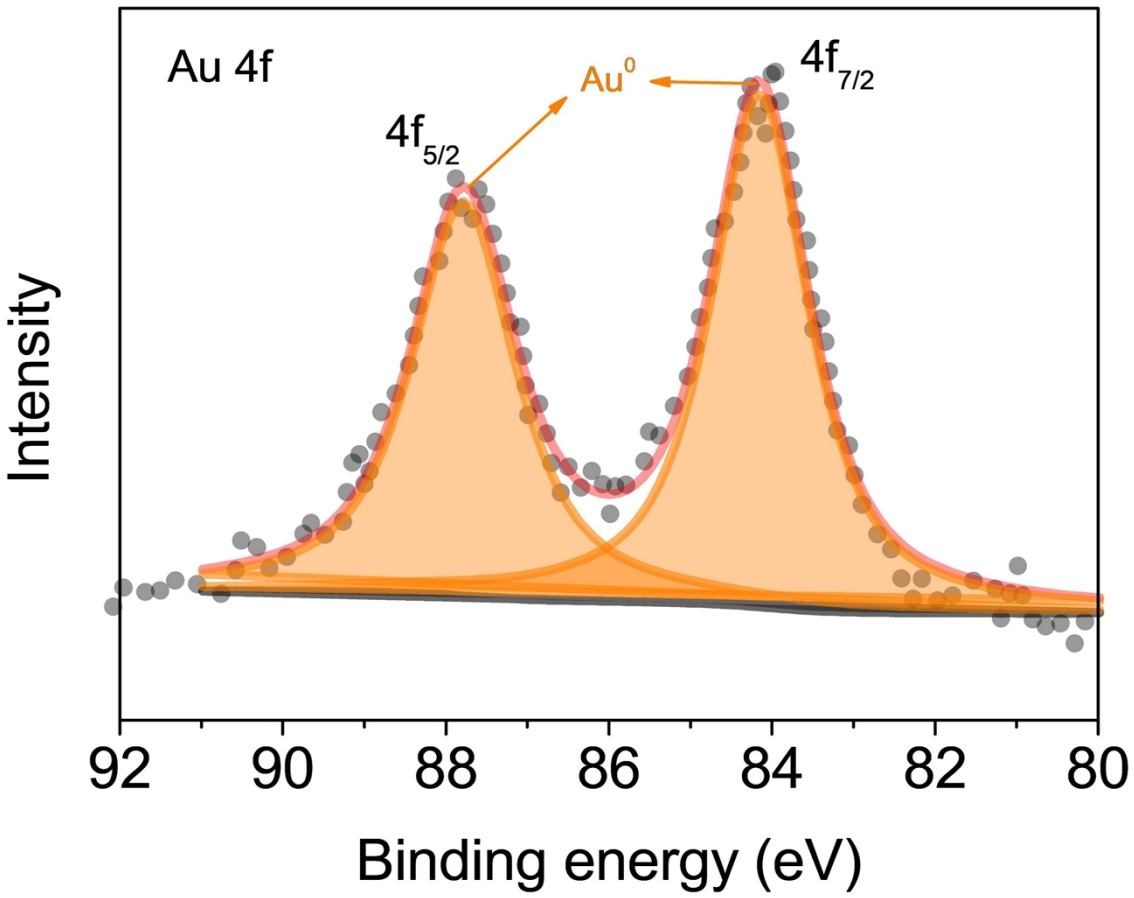

Fig. S9 Au 4f XPS core-level spectra of Au-Pd/HsGDY.

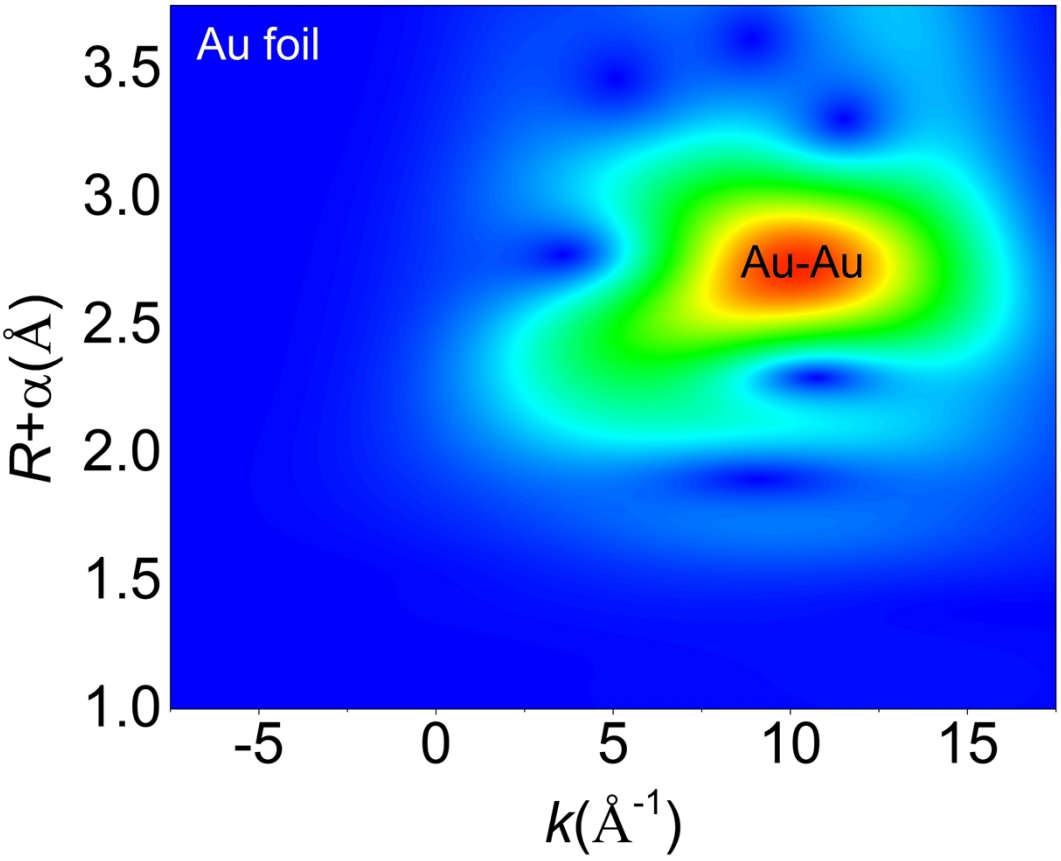

Fig. S10 WT-EXAFS plots of Au L3 edge in Au foil.

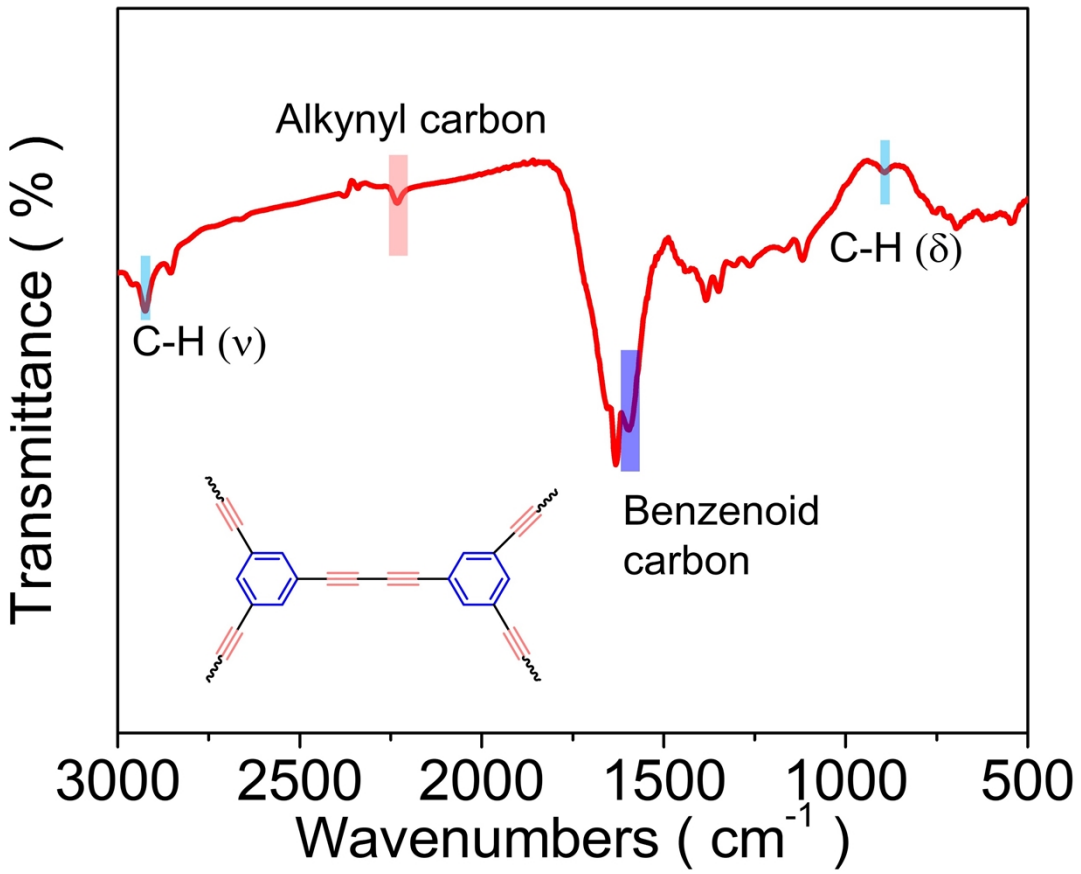

Fig. S11 FT-IR spectrum of Au-Pd/HsGDY.

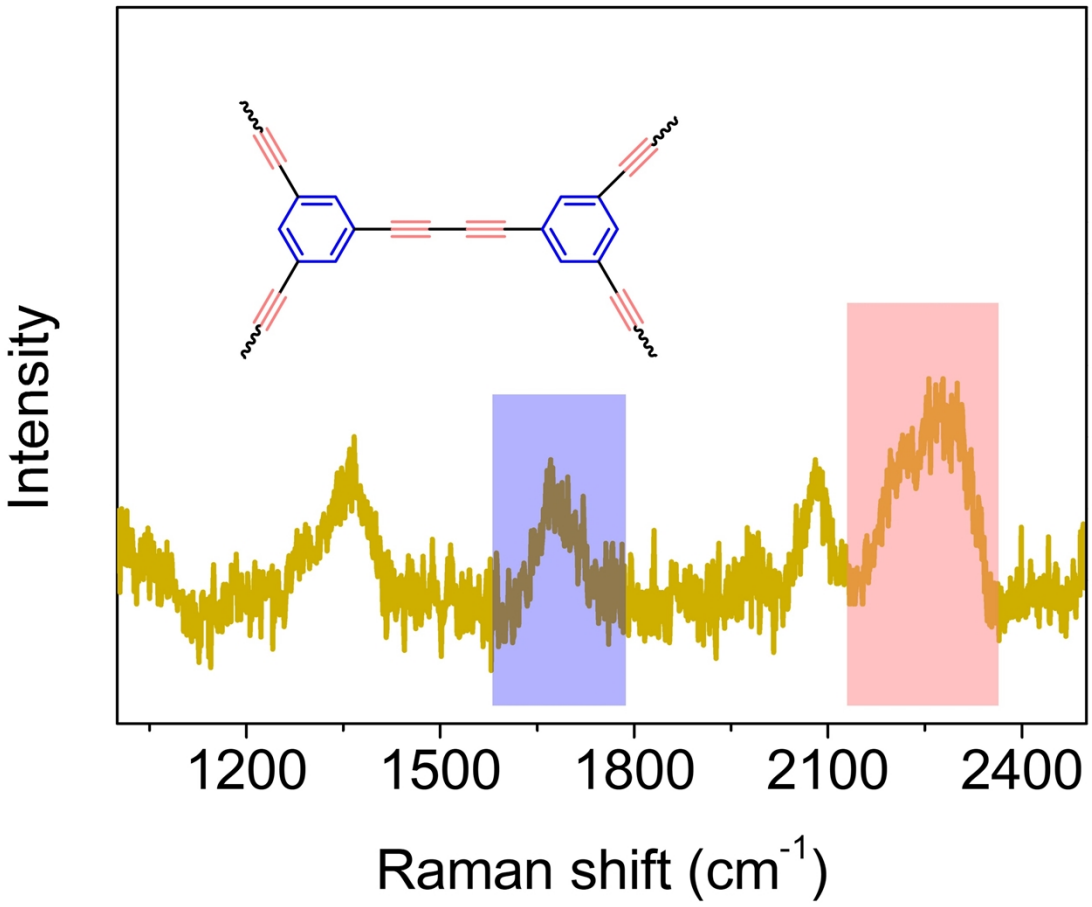

Fig. S12 Raman spectrum of Au-Pd/HsGDY.

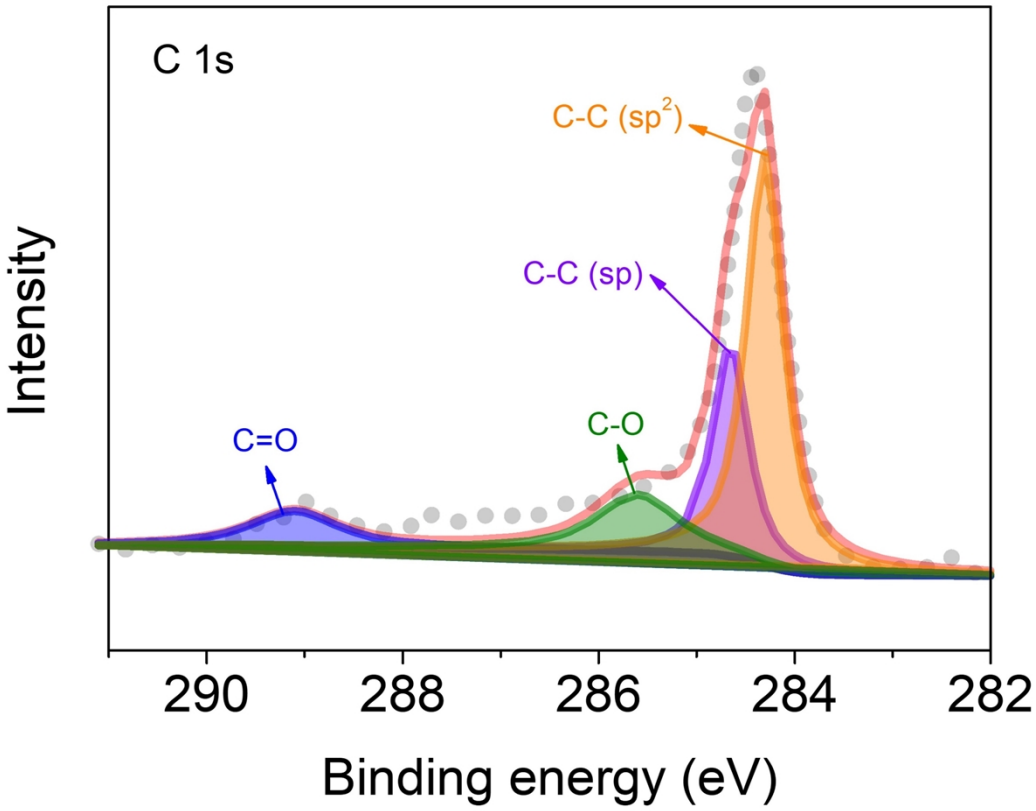

Fig. S13 C 1s core-level XPS spectrum of Au-Pd/HsGDY.

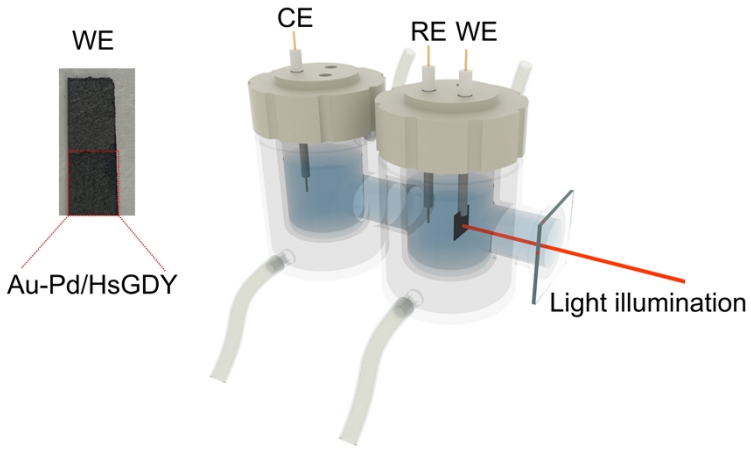

Fig. S14 Schematic of the cell set up, where WE, RE and CE represent the working, reference, and counter electrodes, respectively. The water inlet and outlet were used to adjust the cell temperature during the thermal-control experiments. The red dot rectangle is the area loaded with Au-Pd/HsGDY catalyst.

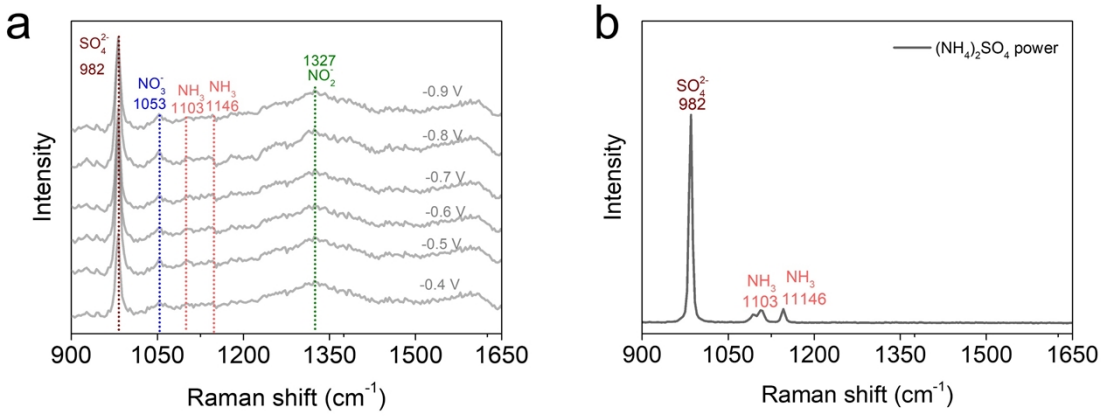

Fig. S15 a) In-situ Raman spectra of the electrode consisting of Au-Pd/HsGDY on carbon cloth at various potentials. b) Raman spectrum of $(NH_4)_2SO_4$.

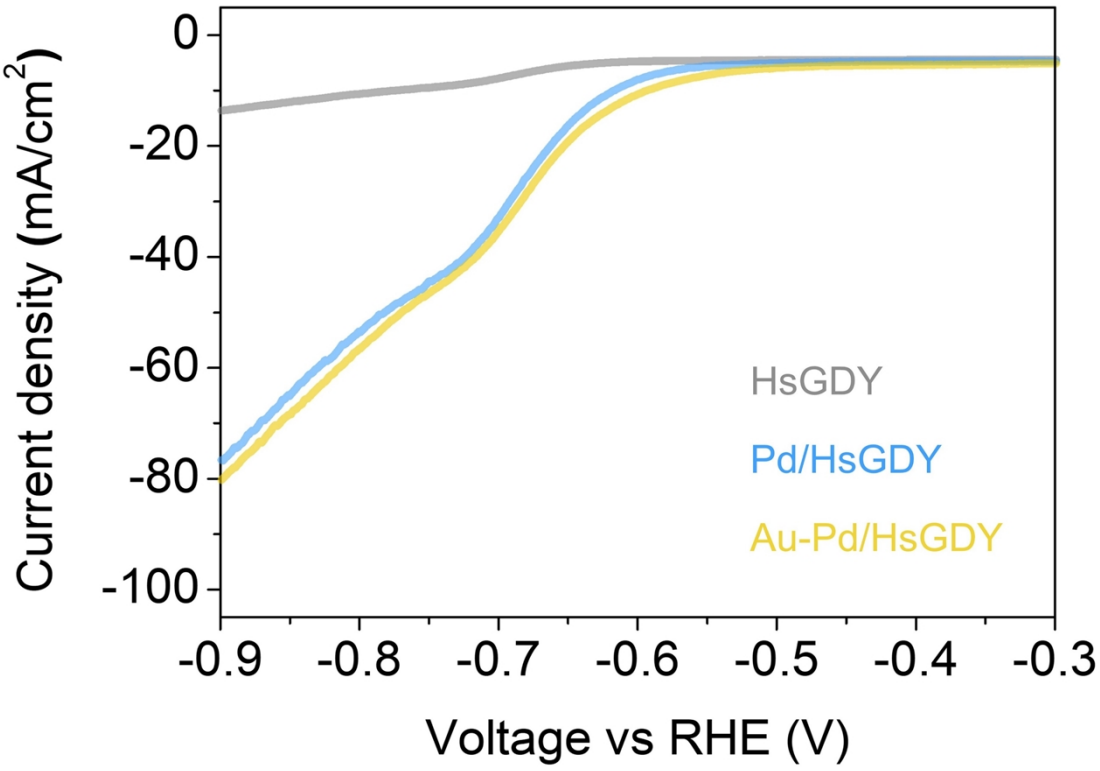

Fig. S16 Linear sweep voltammetry (LSV) curves of the electrodes containing HsGDY, Pd/HsGDY and Au-Pd/HsGDY in the NO_3^- electrolyte.

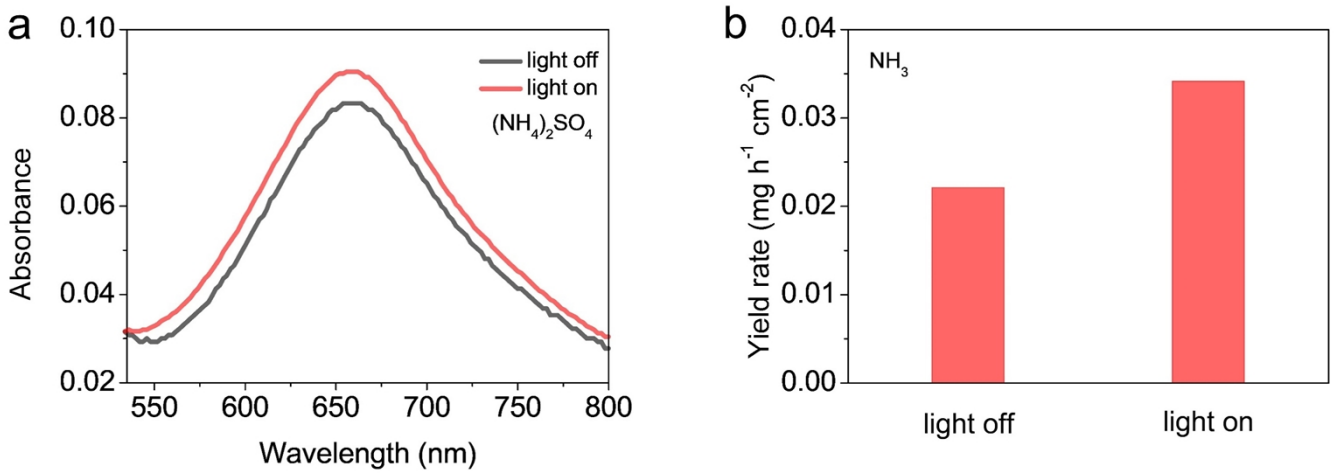

Fig. S17 a) The UV-Vis absorption spectra of the electrolytes after electrochemical nitrate reduction on the Au /HsGDY at -0.6 V and colorimetric reaction using the indophenol blue method. b) The yield rates of NH_3 with light switched on and off.

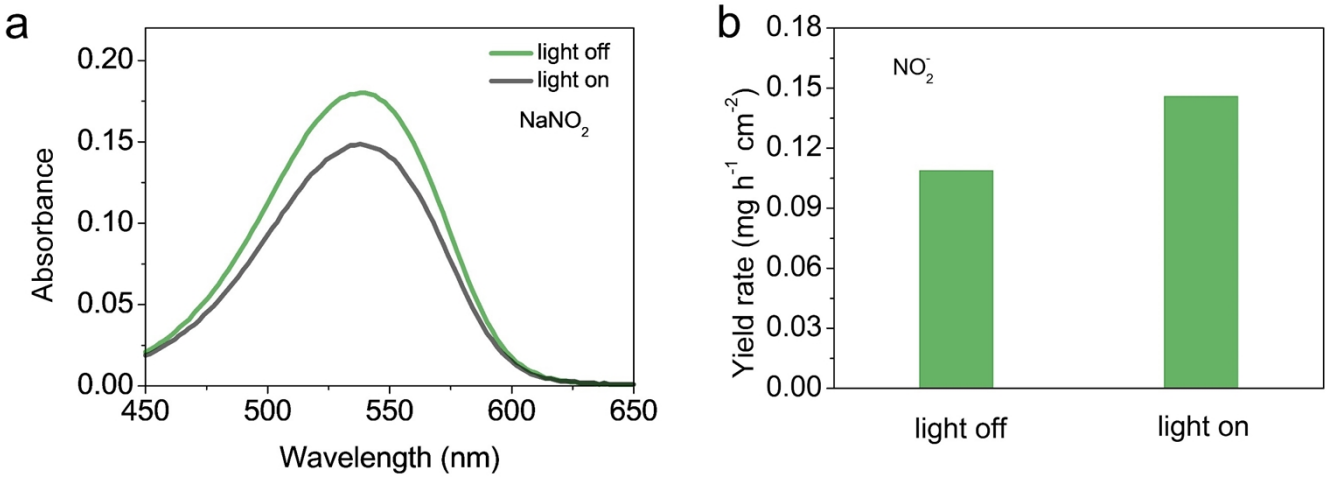

Fig. S18 a) The UV-Vis absorption spectra of the electrolytes after electrochemical nitrate reduction on the Au /HsGDY at -0.6 V and colorimetric reaction using the Griess test. b) The yield rates of NO_2^- with light switched on and off.

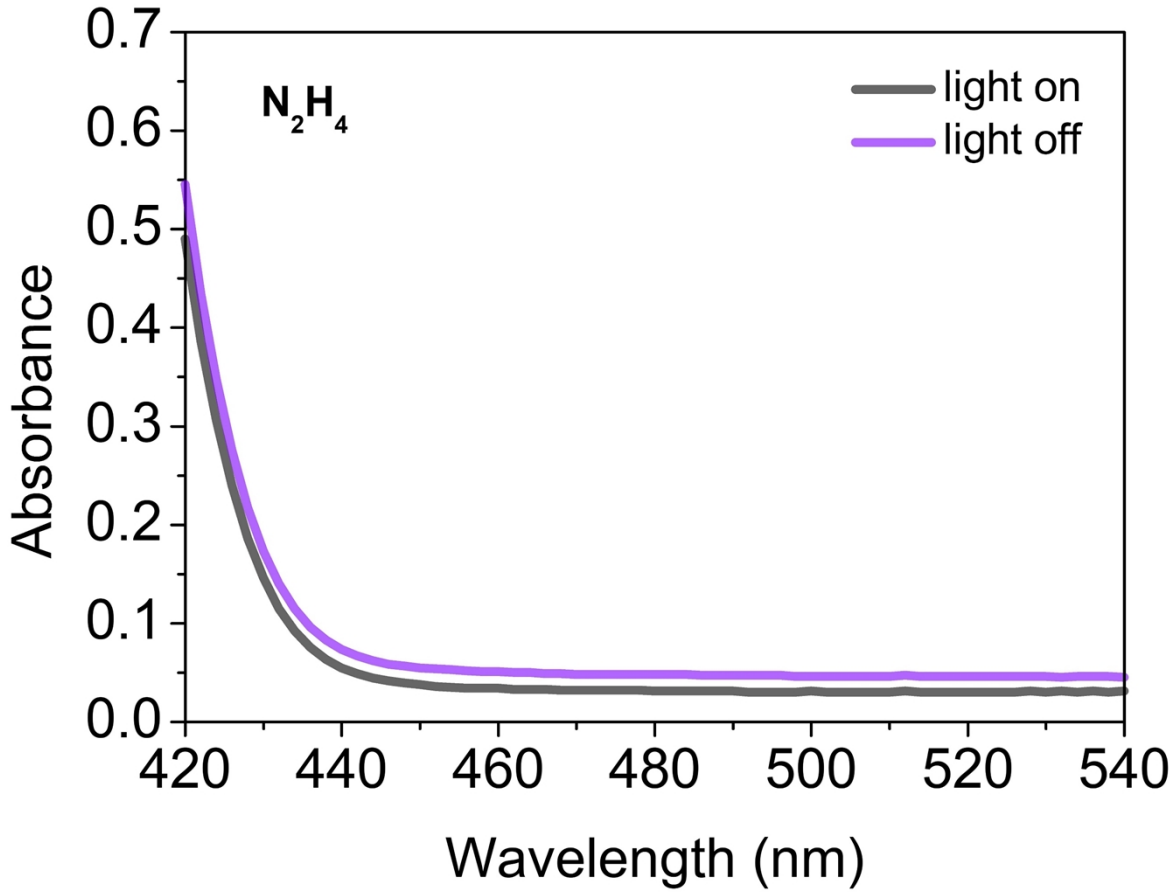

Fig. S19 a) The UV-Vis absorption spectra of the electrolytes after electrochemical nitrate reduction on the Au/HsGDY at -0.6 V and colorimetric reaction using the Watt and Chrisp's method.

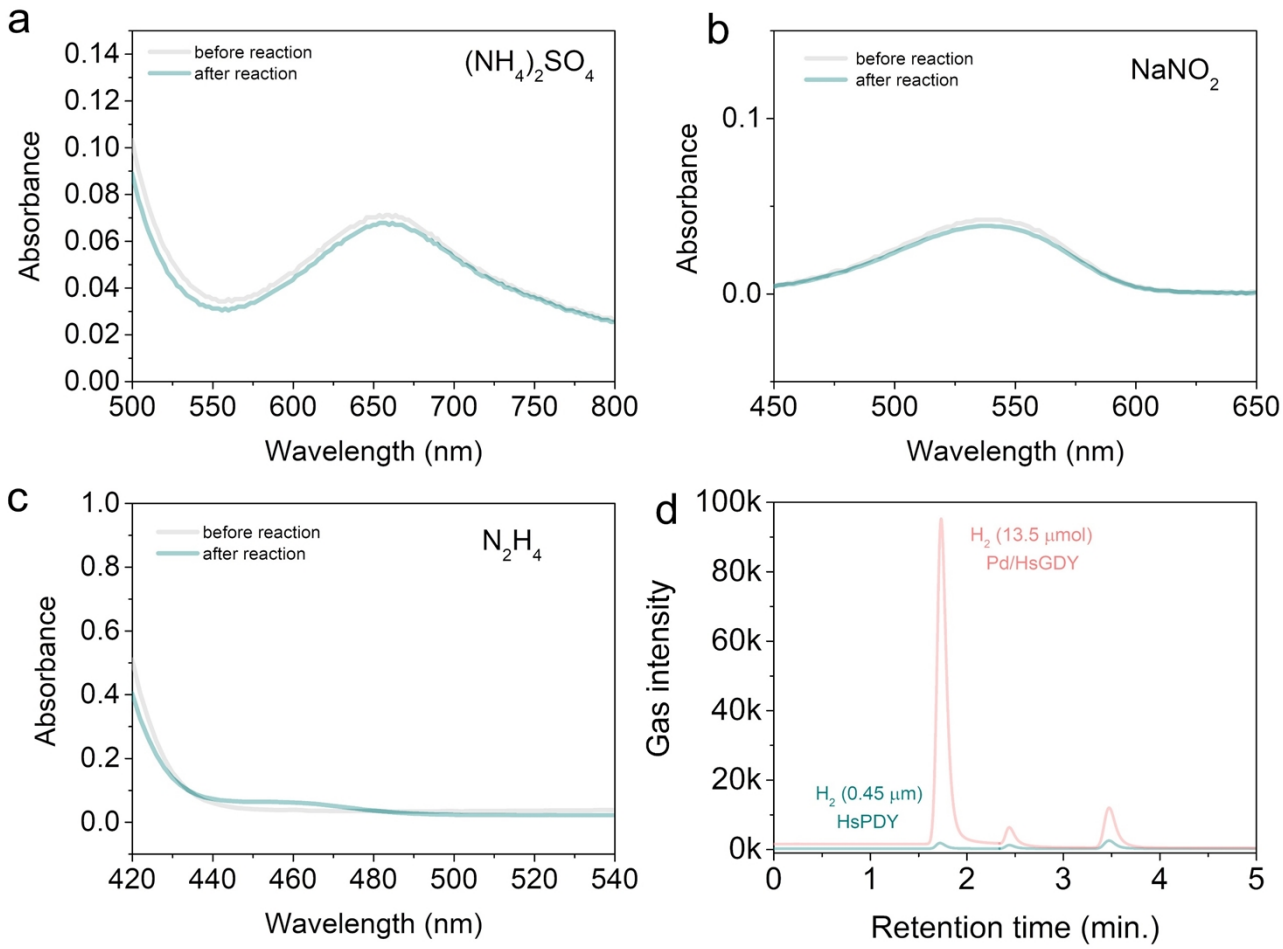

Fig. S20 Determination of the (a) NH_3, (b) NO_3^- , and (c) N_2H_4 in the electrolyte by colorimetric methods when the bare HsGDY electrode were used at -0.7 V. (d) The H_2 generated when nitrate reduction took place on the Pd/HsGDY and the bare HsGDY electrode at -0.7 V.

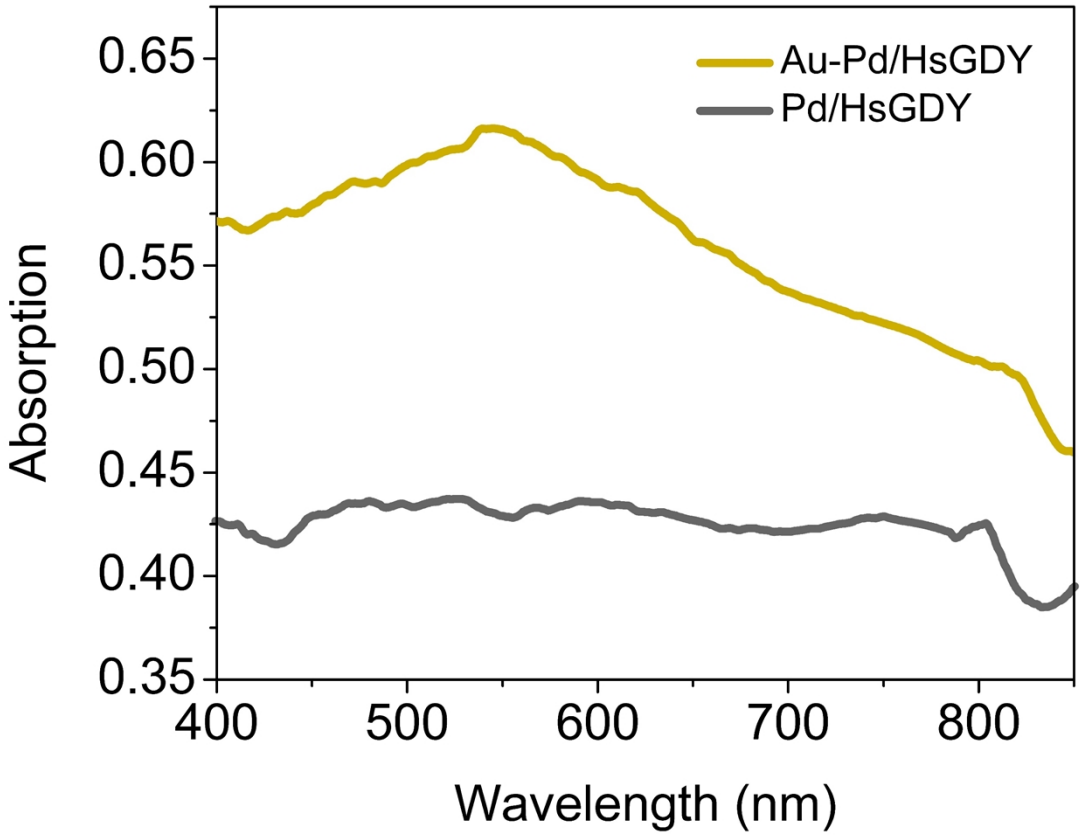

Fig. S21 UV-vis absorption spectra of Au-Pd/HsGDY and Pd/HsGDY.

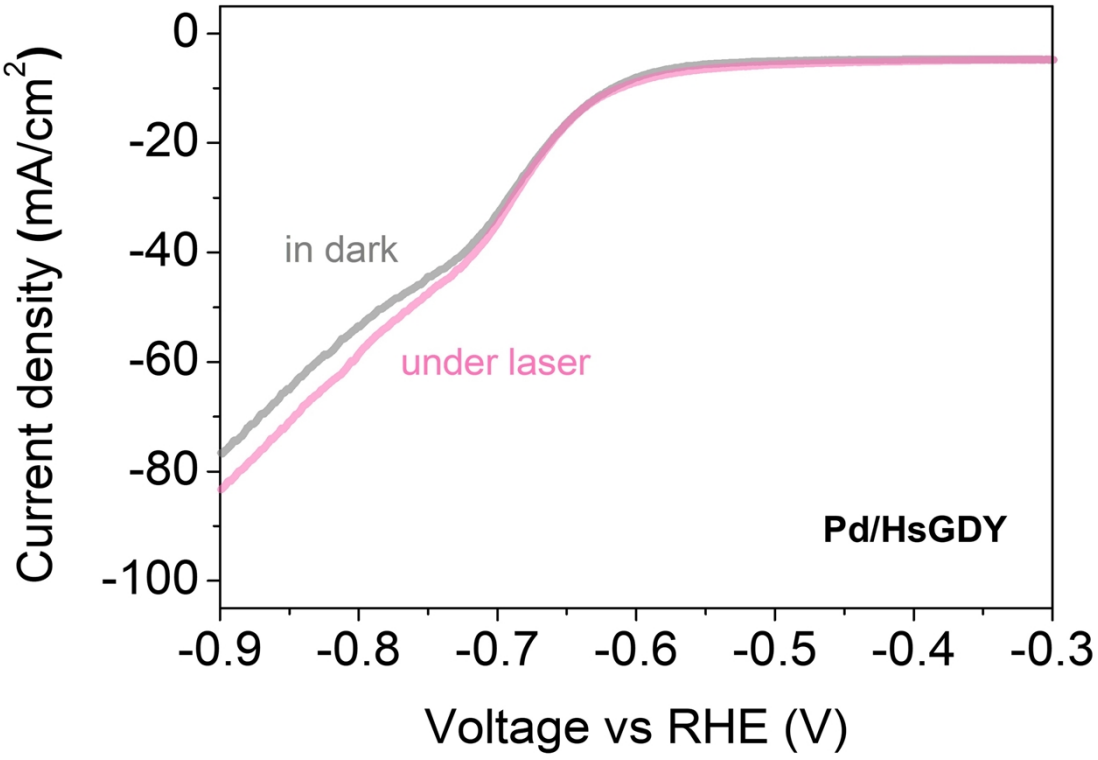

Fig. S22 Linear sweep voltammetry (LSV) curves of the Pd/HsGDY electrode in the NO_3^- electrolyte with light switched on and off.

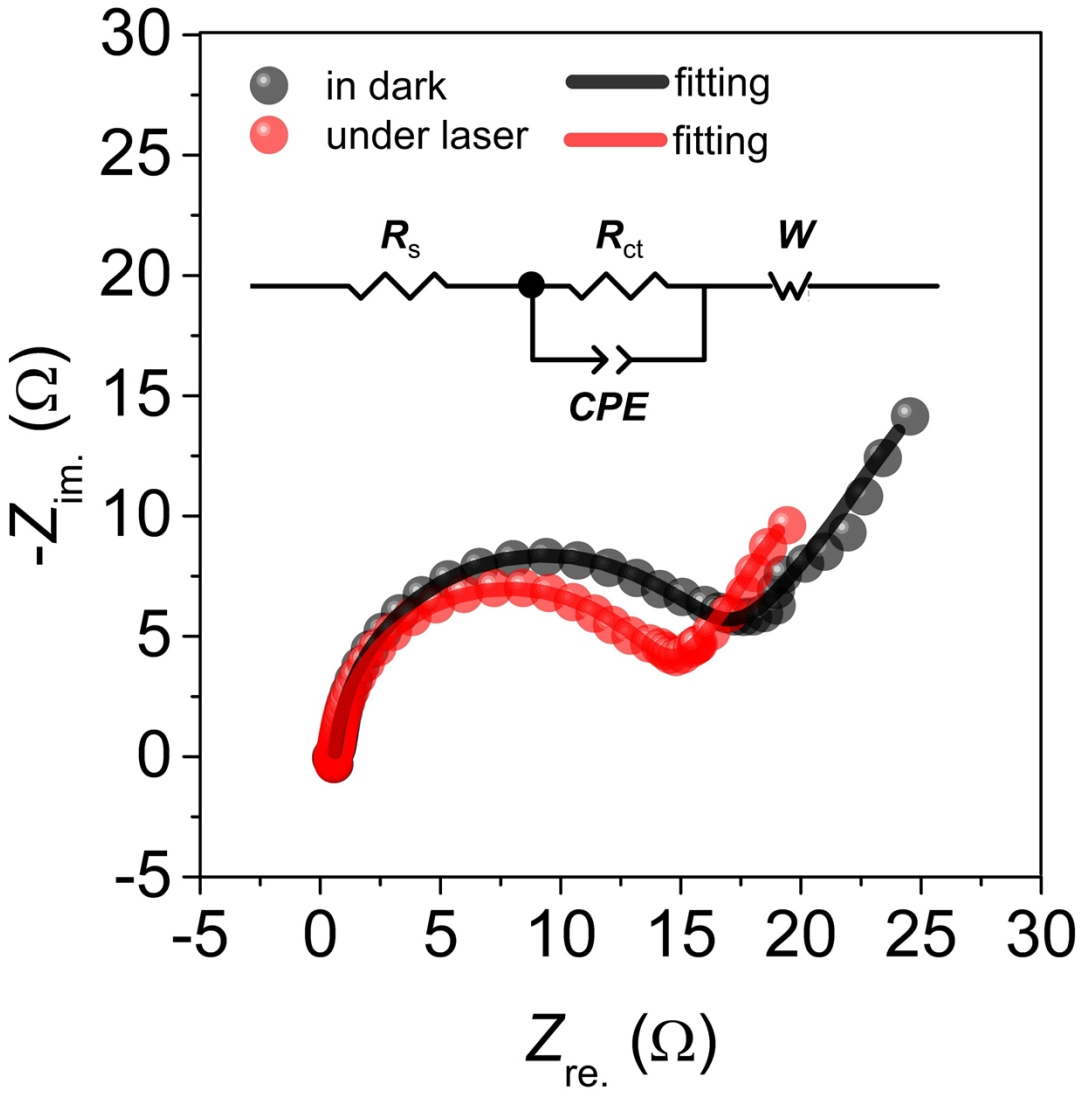

Fig. S23 Nyquist plots of electrochemical impedance spectra of the Au-Pd/HsGDY electrode in the NO_3^- electrolyte with light switched on and off. The electrical equivalent circuit was shown in the inset, where R_s, R_{ct}, CPE and ***W*** represent the electrolyte resistance, charge transfer process, the impedance of the double layer, the diffusional impedance, respectively[12, 13]

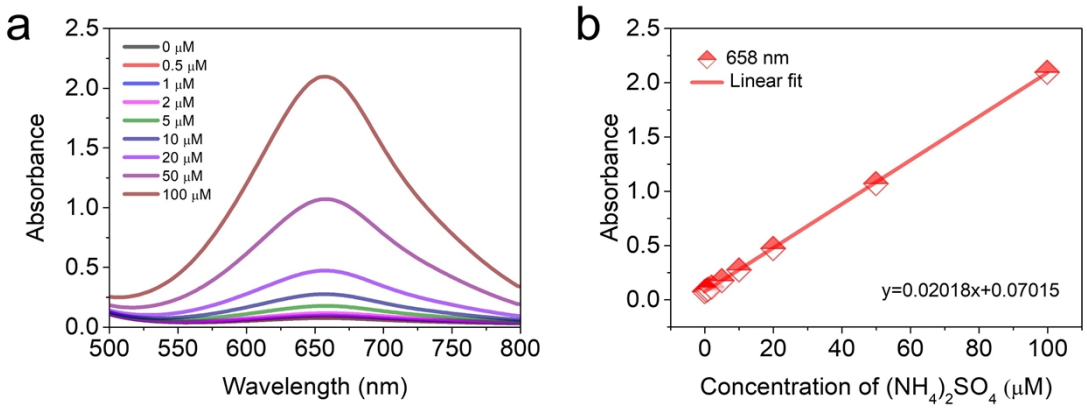

Fig. S24 Determination of the NH_3 using the indophenol blue method. (a) The UV-vis absorption spectra of $(NH4)_2SO_4$ standard solutions with a series of concentrations. (b) The peak intensity at 658 nm as a function of $(NH4)_2SO_4$ concentration established from (a) and the corresponding linear fitting result.

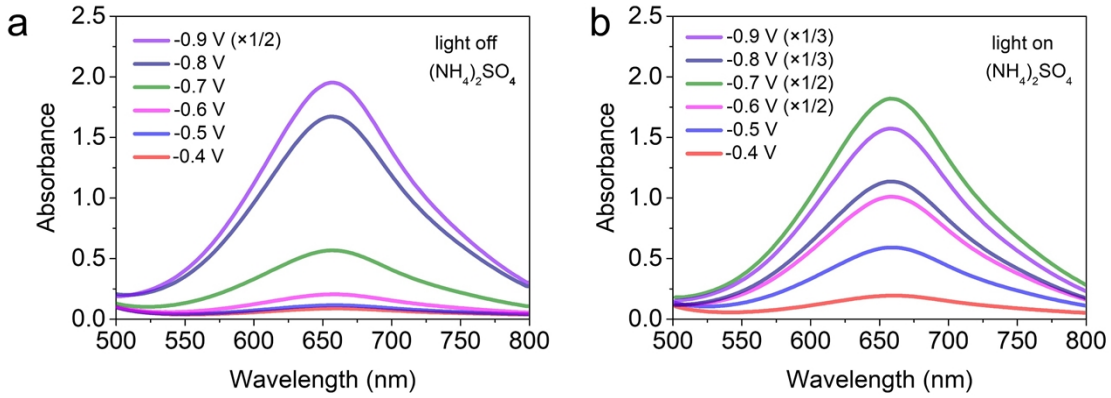

Fig. S25 The UV-Vis absorption spectra of the electrolytes after electrochemical nitrate reduction at varied potentials with light (a) on and (b) off and colorimetric reaction using the indophenol blue method. The fractional number in parentheses refers to the dilution factor.

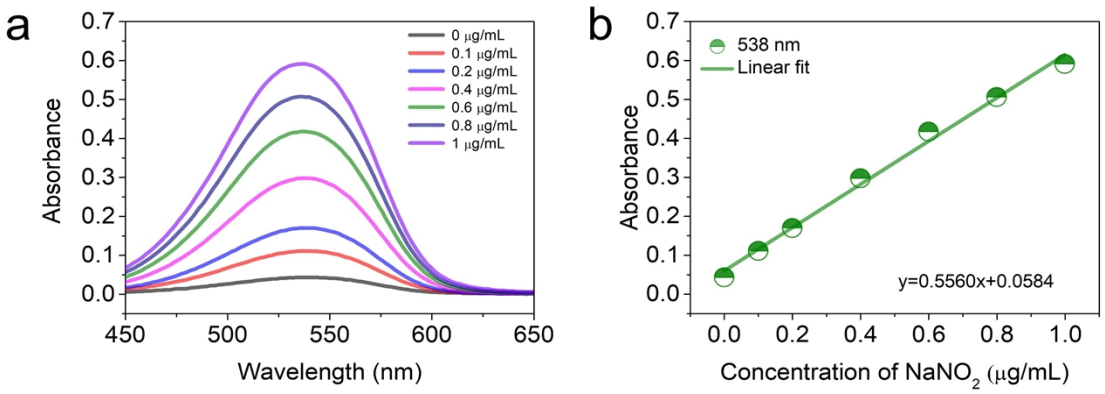

Fig. S26 Determination of the NO_2^- using the Griess test. (a) The UV-Vis absorption spectra of $NaNO_2$ standard solutions with a series of concentrations. (b) The peak intensity at 538 nm as a function of $NaNO_2$ concentration established from (a) and the corresponding linear fitting result.

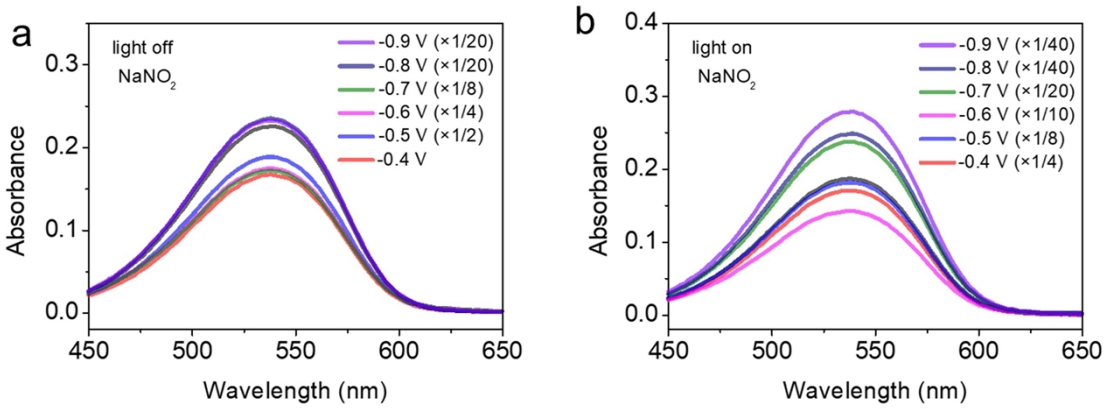

Fig. S27 The UV-Vis absorption spectra of the electrolytes after electrochemical nitrate reduction at varied potentials with light (a) on and (b) off and colorimetric reaction using the Griess test. The fractional number in parentheses refers to the dilution factor.

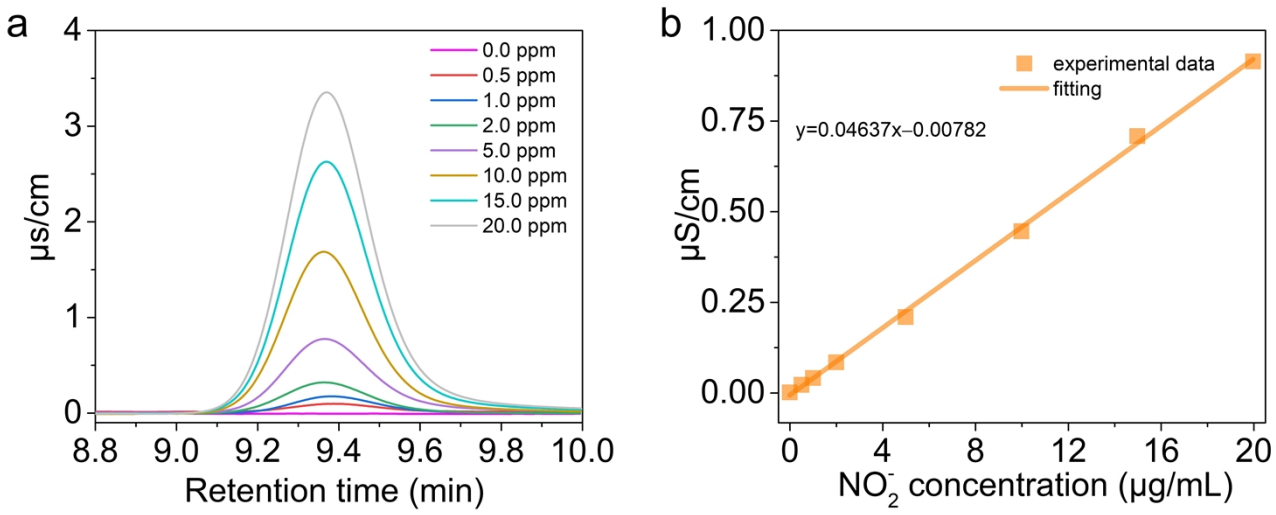

Fig. S28 Determination of the NO_2^- using ion chromatography. (a) The ion chromatography spectra of $NaNO_2$ standard solutions with a series of concentrations. (b) The peak areas centered at 9.39 min as a function of $NaNO_2$ concentration established from (a) and the corresponding linear fitting result.

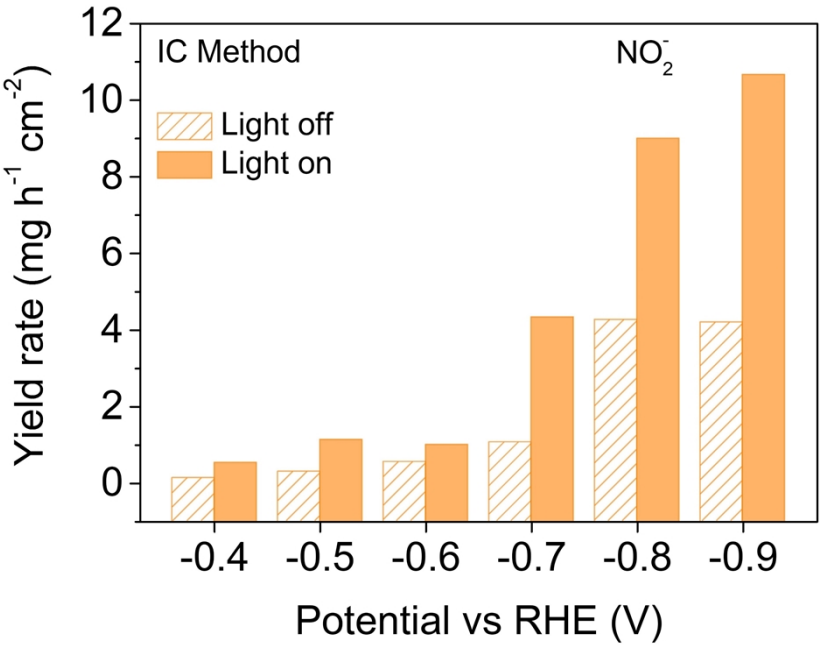

Fig. S29 Potential-dependent yield rate of NO_2^- with light switched on and off, which is measured by IC method.

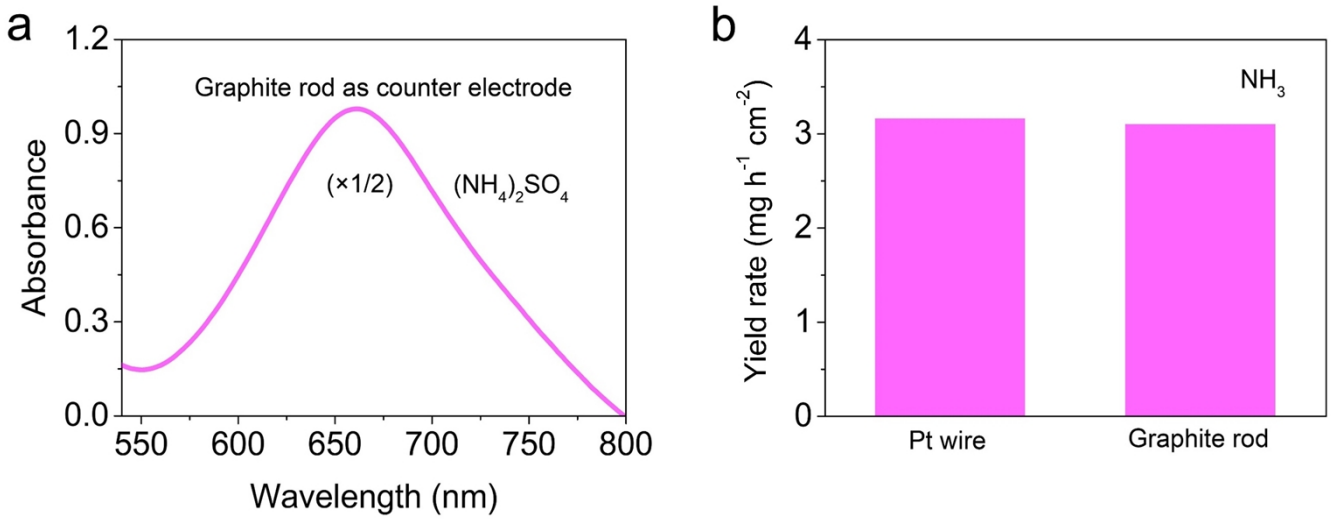

Fig. S30 a) The UV-Vis absorption spectra of the electrolyte after electrochemical nitrate reduction at -0.6 V with graphite rod as counter electrode under illumination of white light for 30 min, and colorimetric reaction using the indophenol blue method. The fractional number in parentheses refers to the dilution factor. b) The comparison of yield rate of NH_3 using Pt wire and graphite rod as counter electrode.

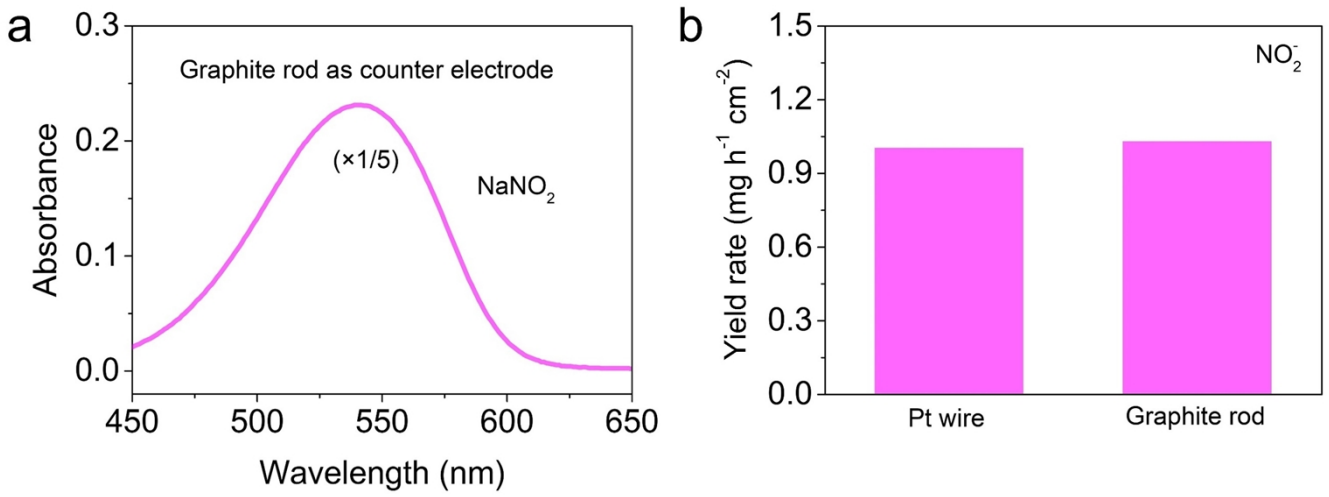

Fig. S31 a) The UV-Vis absorption spectra of the electrolyte after electrochemical nitrate reduction at -0.6 V with graphite rod as counter electrode under illumination of white light for 30 min, and colorimetric reaction using by the Griess test. The fractional number in parentheses refers to the dilution factor. b) The comparison of yield rate of NO_2^- using Pt wire and graphite rod as counter electrode.

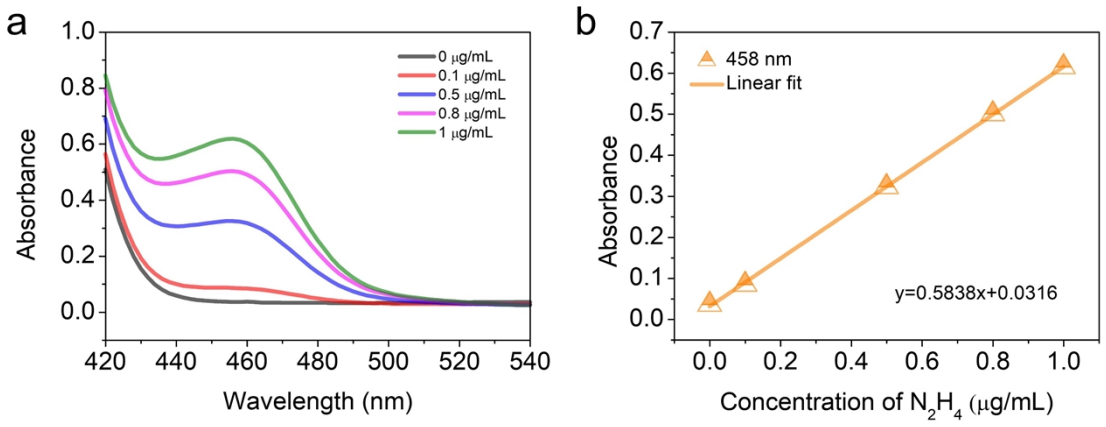

Fig. S32 Determination of the N_2H_4 using the Watt and Chrisp's method. (a) The UV-Vis absorption spectra of N_2H_4 standard solutions with a series of concentrations. (b) The peak intensity at 458 nm as a function of N_2H_4 concentration established from (a) and the corresponding linear fitting result.

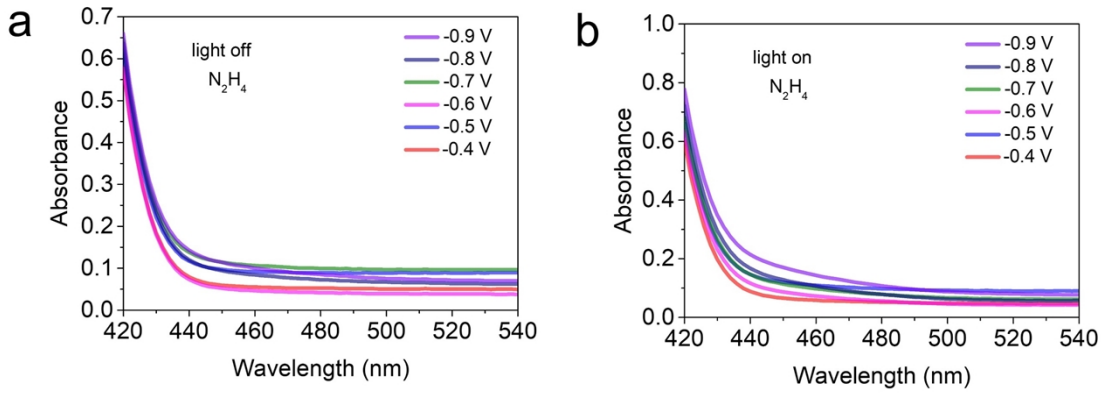

Fig. S33 The UV-Vis absorption spectra of the electrolytes after electrochemical nitrate reduction at varied potentials with light (a) on and (b) off and colorimetric reaction using the Watt and Chrisp's method.

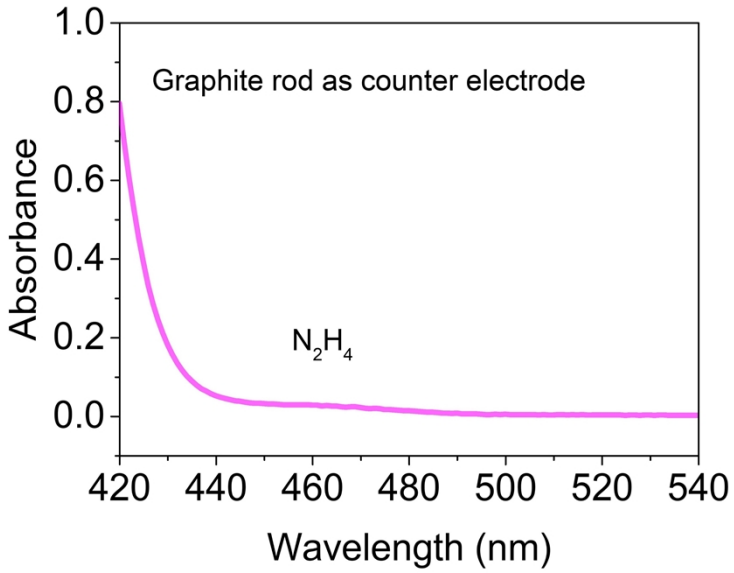

Fig. S34 The UV-Vis absorption spectra of the electrolyte after electrochemical nitrate reduction at -0.6 V with graphite rod as counter electrode under illumination of white light for 30 min, and colorimetric reaction using the Watt and Chrisp's method.

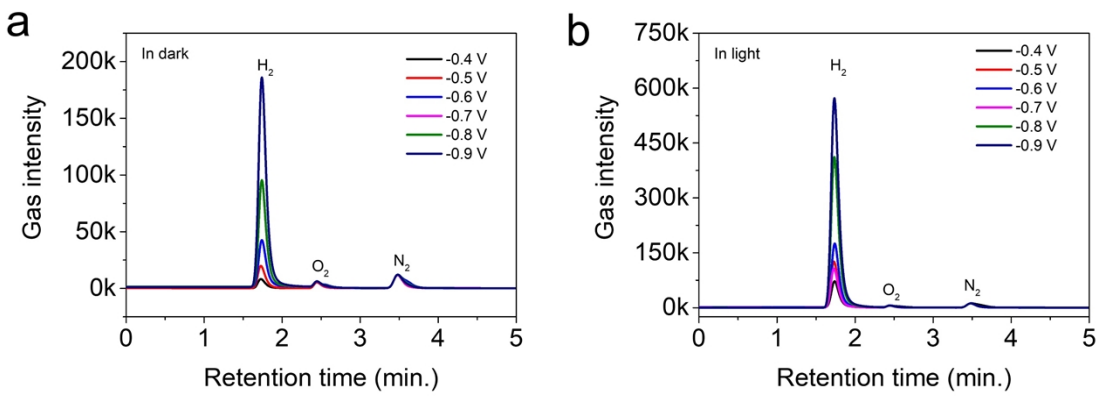

Fig. S35 Determination of the H_2 produced alongside electrochemical nitrate reduction at varied potentials using gas chromatography.

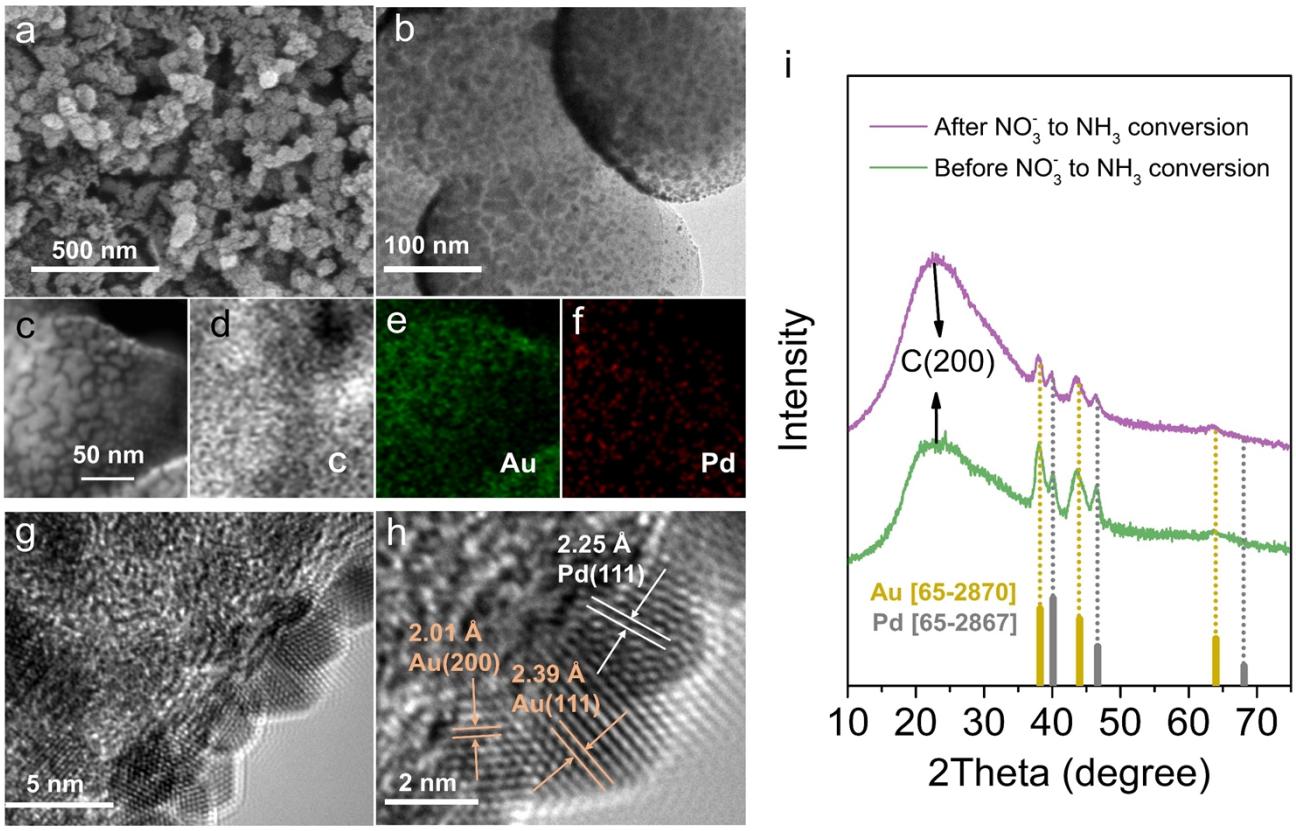

Fig. S36 The morphological and structural characterization of Au-Pd/HsGDY after NO_3^--to-NH_3 conversion at -0.6 V under plasmonic excitation. a) SEM, b) TEM, c) HAADF-STEM images, and d-f) corresponding EDS mapping of C, Au and Pd. g, h) High resolution TEM images with the lattice plane distances of Au and Pd nanoparticles marked by gold and white lines, respectively. i) XRD patterns of Au- Pd/HsGDY before and after plasmonic electrocatalysis, with the dot lines added for convivence of peaks assignment.

.

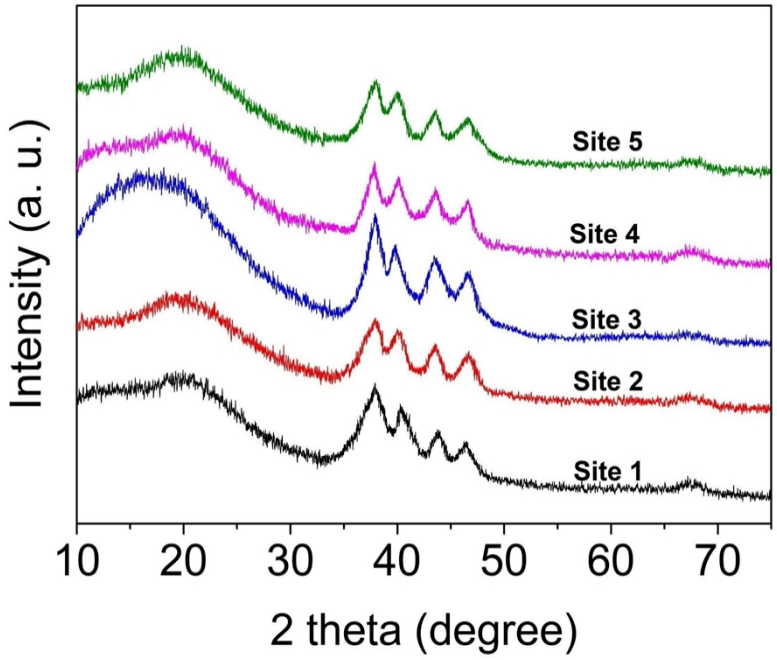

Fig. S37 XRD patterns of the as-prepared working electrode collected from five different sites

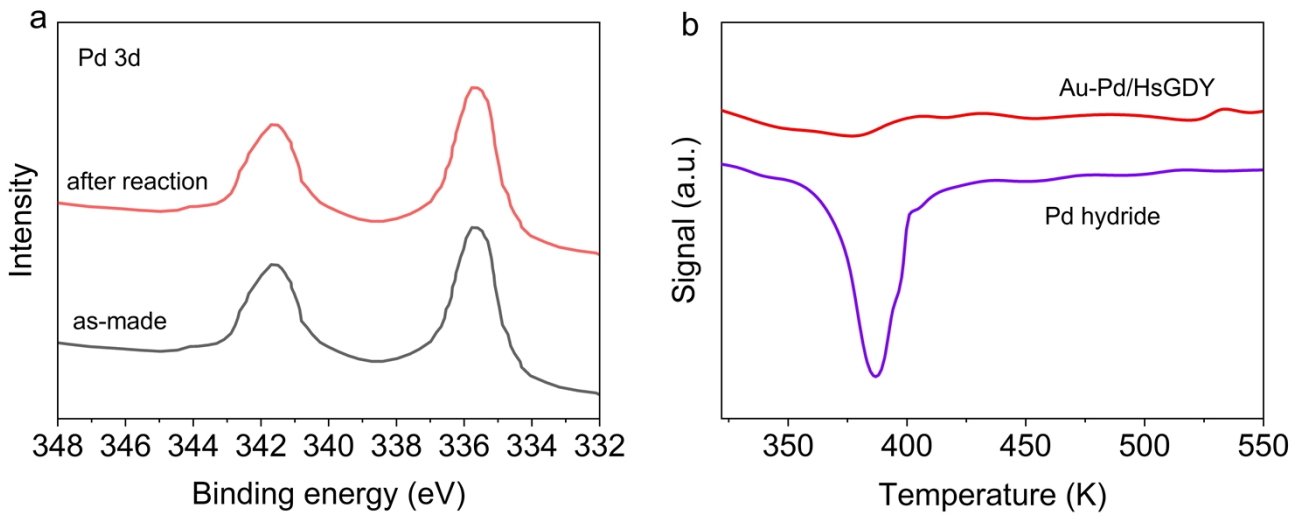

Fig. S38 a) Pd 3d core-level X-ray photoelectron spectrum (XPS) of as-made Au-Pd/HsGDY and that after the electrochemical reduction of NO_3- at -0.6 V for 30 min. b) TPR profiles of Au-Pd/HsGDY after the electrochemical reduction of NO3- and Pd hydride.

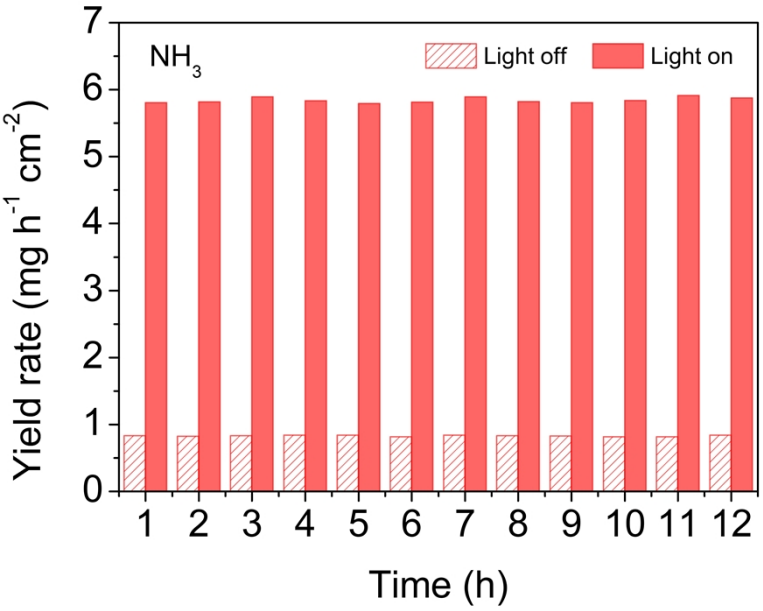

Fig. S39 Time-dependent yield rate of NH_3 for electrochemical reduction of NO_3^- executing on Au-Pd/HsGDY electrode with light switched on and off.

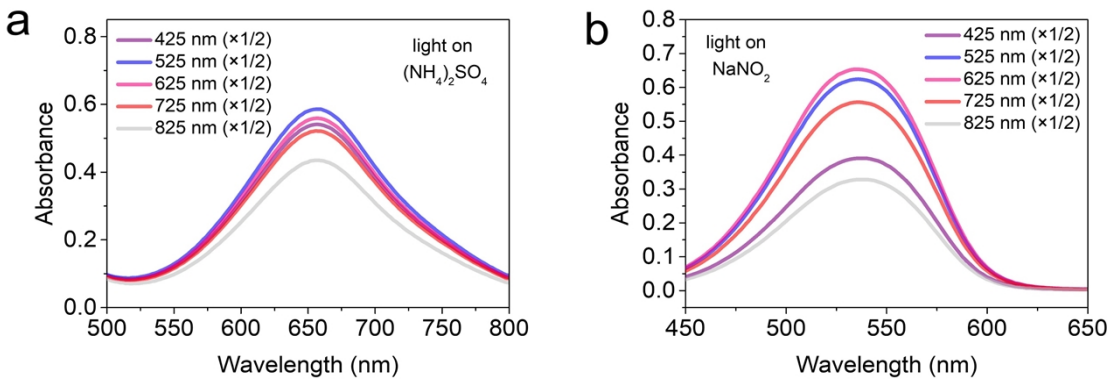

Fig. S40 The UV-Vis absorption spectra of the electrolytes after electrochemical nitrate reduction at -0.6 V under light illumination of different wavelength and colorimetric reaction using the indophenol blue method.

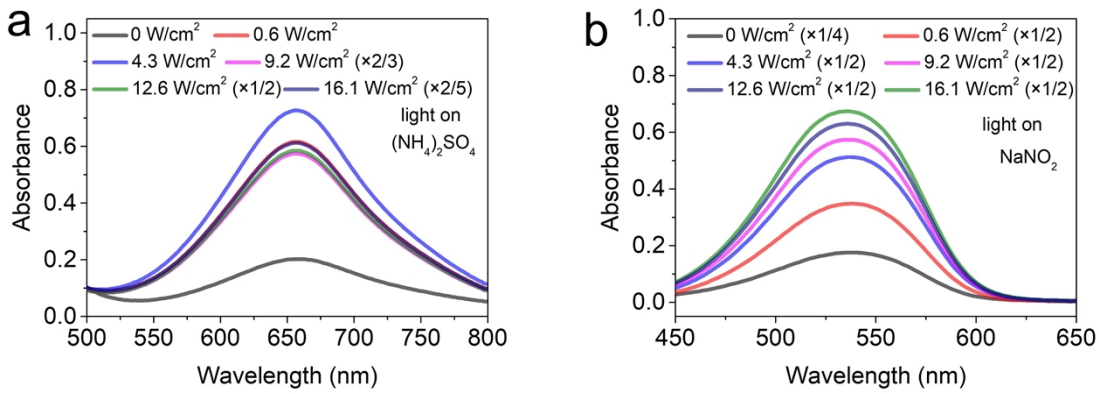

Fig. S41 The UV-Vis absorption spectra of the electrolytes after electrochemical nitrate reduction at -0.6 V under light illumination of different intensity and colorimetric reaction using by the Griess test.

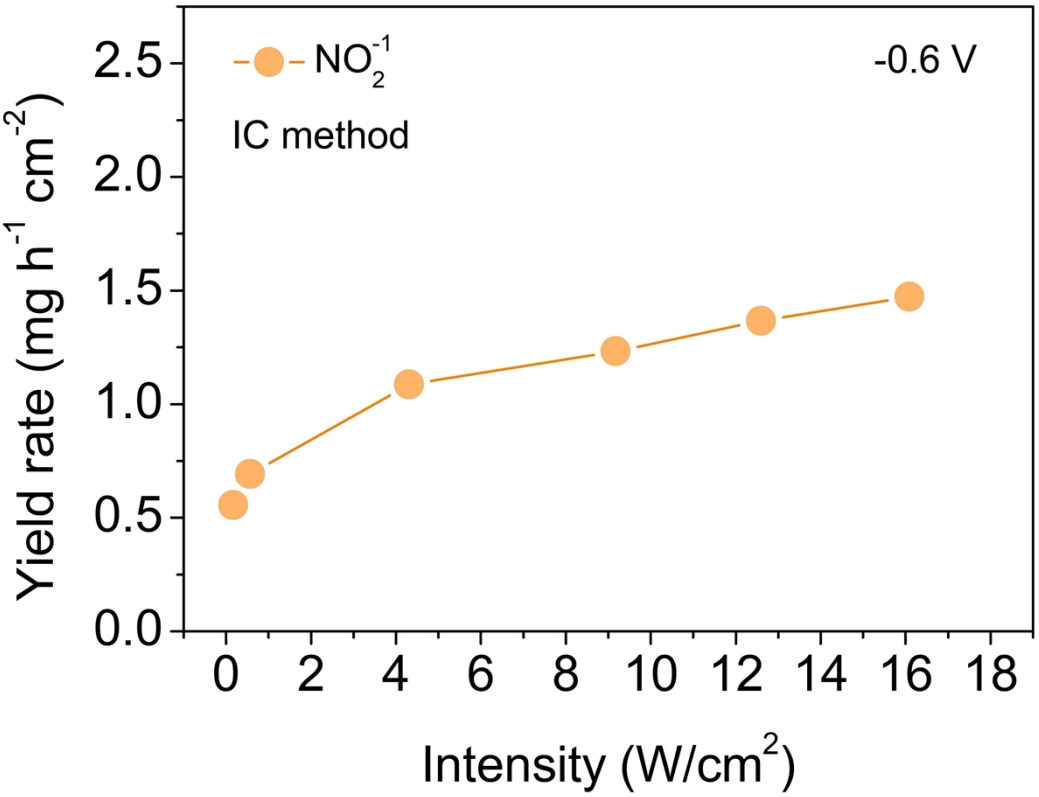

Fig. S42 Light intensity-dependent yield rate of NO_2^-, which is measured by IC method.

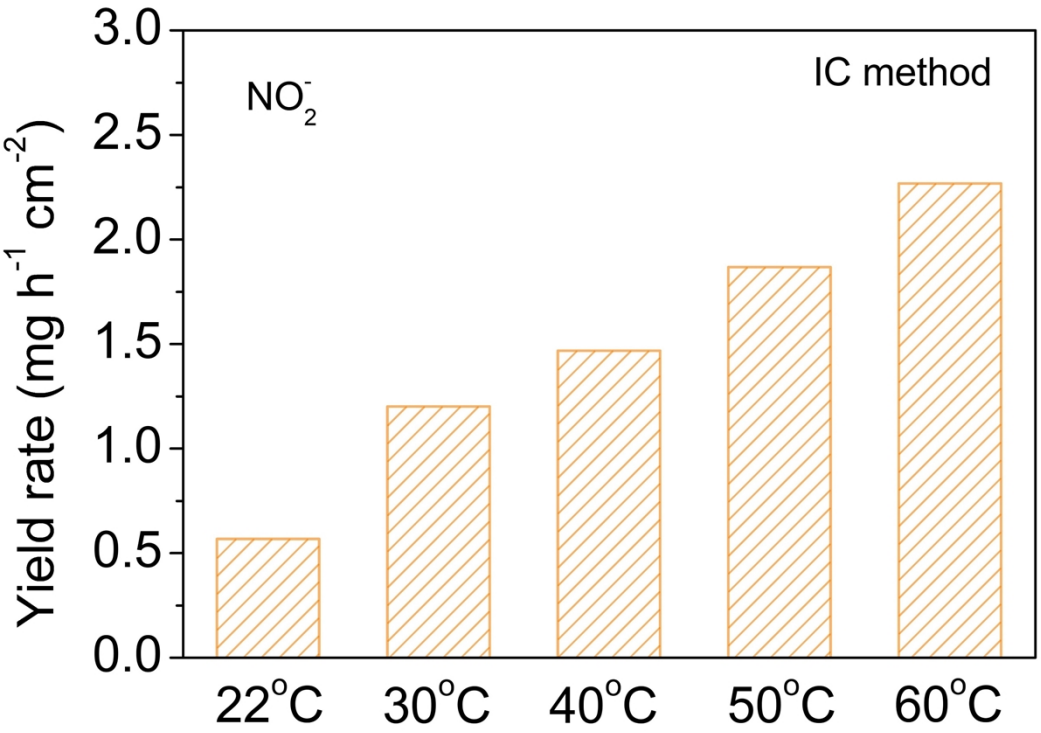

Fig. S43 Temperature -dependent yield rate of NO_2^-, which is measured by IC method.

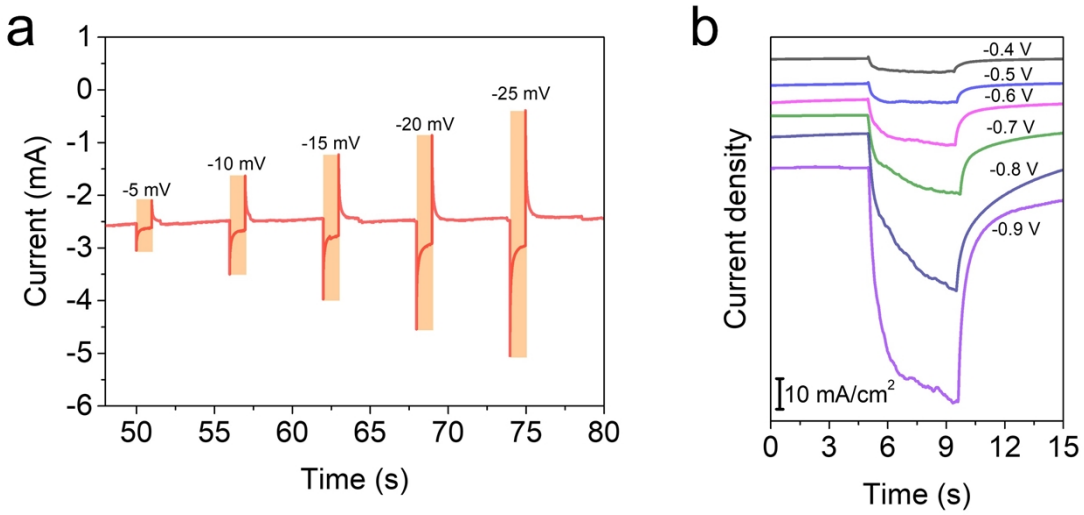

Fig. S44 (a) Chronoamperometric curves of the Au-Pd/HsGDY electrode generated by superimposing different indicated voltage pulse at −0.6 V. (b) Chronoamperometric curves of the Au-Pd/HsGDY electrode at -0.6 V with white-light (135.1Wcm^{-2}) switched on/off. The lines were offset for clarity with the corresponding current scales shown in the bottom left corner.

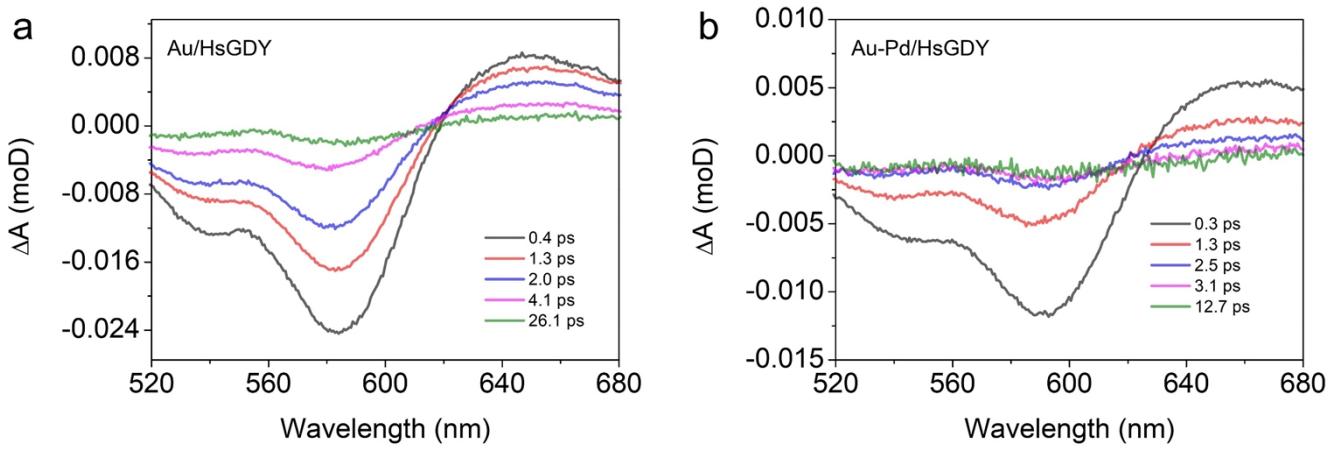

Fig. S45 a, b) Ultrafast TA spectroscopy of Au/HsGDY and Au-Pd/HsGDY recorded with a 500 nm pump.

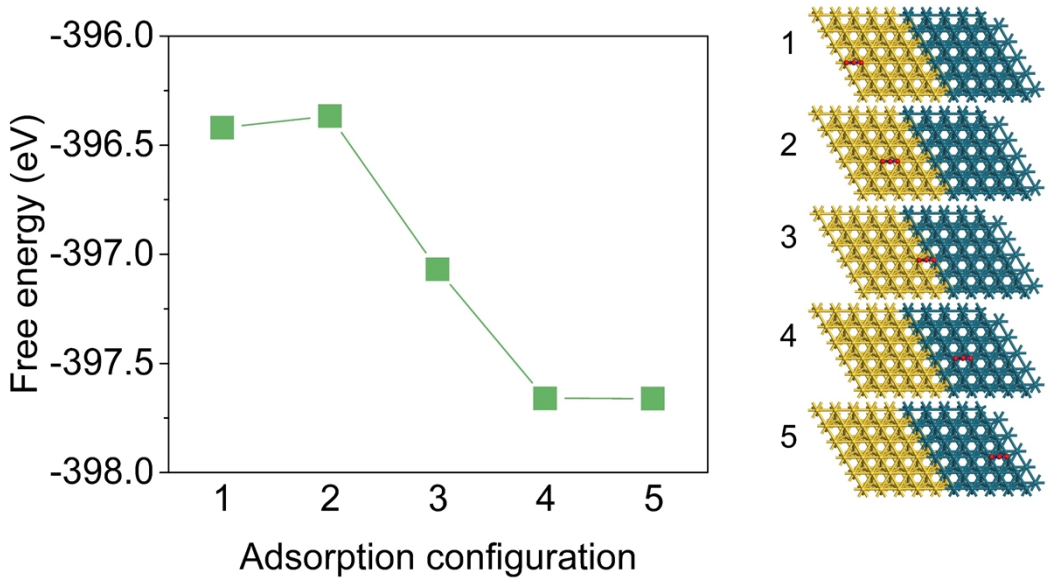

Fig. S46 Static free-energy diagrams of NO_3^- adsorbed on different sites in the Pd_5Au model. The Pd, Au, N, and O atoms are represented by cyan, yellow, blue, red spheres, respectively.

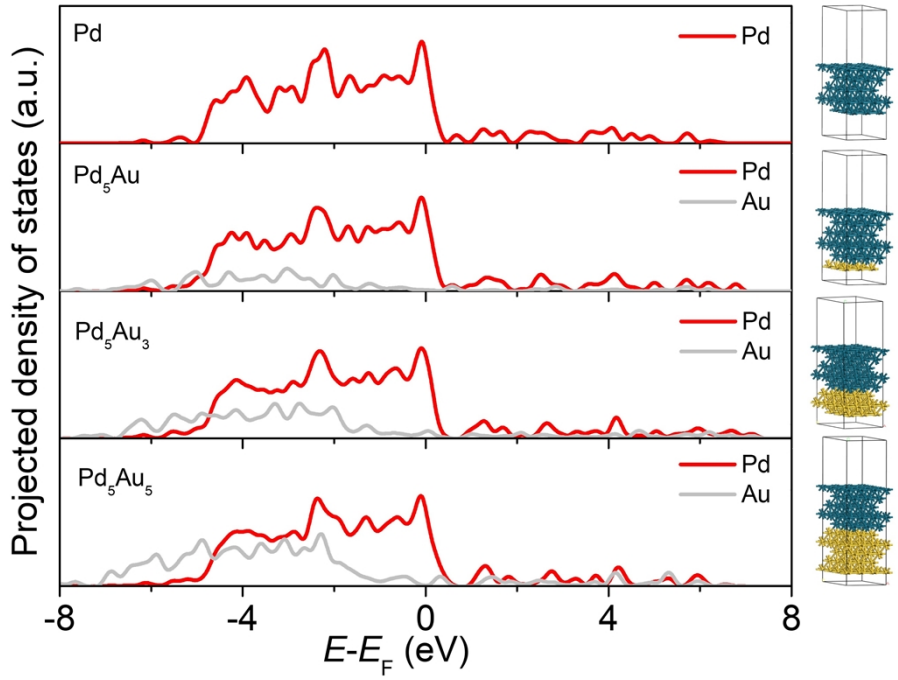

Fig. S47 Projected density of states of Pd_5, Pd_5Au, Pd_5Au_3 and Pd_5Au_5 models. The corresponding structures are illustrated in the right, with the Pd and Au colored by cyan and yellow, respectively.

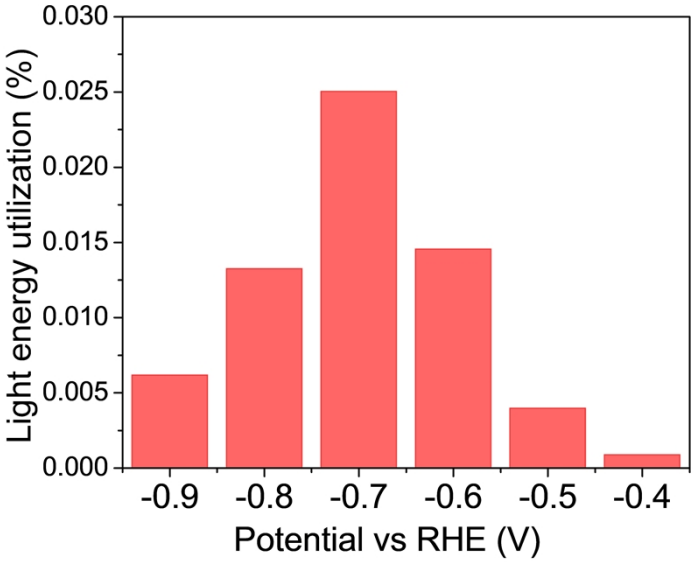

Fig. S48 Potential-dependent utilization of light energy for NO_3^--to-NH_3 electrochemical conversion.

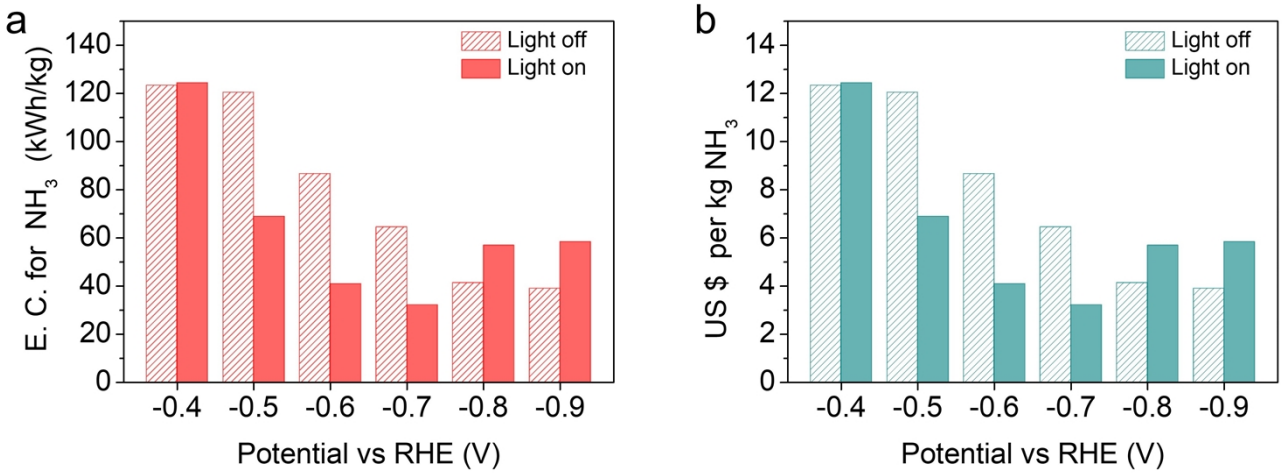

Fig. S49 a) Potential-dependent energy consumption and b) production cost of NH_3.

Table S1. Fitting parameters for the EIS measurement based on the equivalent electrical circuit.

	R_s (Ω)	R_{ct} (Ω)	CPE (F), p	W (Ω)
in dark	0.616	14.62	6.34×10^{-5}, 0.986	87.41
under laser	0.597	12.92	7.522×10^{-5}, 0.973	53.44

Table S2. ICP-MS detemination of Au and Pd ions in the electrolyte after electrochemical reduction of NO_3^- to NH_3 at -0.6 V under laser illumination for 30 min.

Element	Concentration (μg/L)		*n*
	Blank solution	Electrolyte	
^{197}Au	<0.1	<0.1	3
^{106}Pd	<0.1	<0.1	3

Table S3. The DFT calculated adsorption energy ΔE, ΔE_{ZPT}-TΔS and the Gibbs free energy ΔG for various species in the reaction pathways.

	Ground (eV)			Excited (eV)		
	ΔE	$\Delta E_{ZPT} - T\Delta S$	ΔG	ΔE	$\Delta E_{ZPT} - T\Delta S$	ΔG
*+NO_3^-	-	-	0	-	-	-
*NO_3	0.470	0.248	0.718	0.102	0.248	0.350
*NO_2	-1.360	0.160	-1.200	-1.229	0.160	-1.069
*+NO_2^-	-	-	0.932	-	-	-
*NO	-2.861	0.068	-2.793	-1.229	0.046	-2.950
*NOH	-3.345	0.408	-2.937	-3.418	0.376	-3.042
*N	-4.547	0.086	-4.461	-4.843	0.086	-4.757
*NH	-5.200	0.374	-4.826	-5.253	0.374	-4.879
*NH_2	-4.918	0.561	-4.357	-5.014	0.561	-4.453
*NH_3	-6.518	0.949	-5.569	-6.318	0.912	-5.406
*+NH_3	-	-	-5.299	-	-	-

References

1. H.-Y. Sun, Y. Ding, Y.-Q. Yue, Q. Xue, F.-M. Li, J.-X. Jiang, P. Chen and Y. Chen, *ACS Appl. Mater. Interfaces*, 2021, **13**, 13149-13157.
2. P. Li, Z. Jin, Z. Fang and G. Yu, *Environ. Sci. Technol.*, 2021, **14**, 3522-3531.
3. G. Kresse and J. Furthmüller, *Comput. Mater. Sci.*, 1996, **6**, 15-50.
4. G. Kresse and D. Joubert, *Phys. Rev. B*, 1999, **59**, 1758-1775.
5. J. P. Perdew, K. Burke and M. Ernzerhof, *Phys. Rev. Lett.*, 1996, **77**, 3865-3868.
6. H. J. Monkhorst and J. D. Pack, *Phys. Rev. B*, 1976, **13**, 5188-5192.
7. V. Wang, N. Xu, J.-C. Liu, G. Tang and W.-T. Geng, *Comput. Phys. Commun.*, 2021, **267**, 108033.
8. J. Zhao, Y. Bai, Z. Li, J. Liu, W. Wang, P. Wang, B. Yang, R. Shi, G. I. N. Waterhouse, X. D. Wen, Q. Dai and T. Zhang, *Angew. Chem. Int. Ed.*, 2023, **62**, e202219299.
9. J. K. Noerskov, T. Bligaard, A. Logadottir, J. R. Kitchin, J. G. Chen, S. Pandelov and U. Stimming, *ChemInform*, 2005, **36**.
10. F. Calle-Vallejo, M. Huang, J. B. Henry, M. T. M. Koper and A. S. Bandarenka, *Phys. Chem. Chem. Phys.*, 2013, **15**, 3196-3202.
11. J.-X. Liu, D. Richards, N. Singh and B. R. Goldsmith, *ACS Catal.*, 2019, **9**, 7052-7064.
12. W. Ou, Y. Fan, J. Shen, Y. Xu, D. Huang, B. Zhou, T. W. Lo, S. Li, Y. Y. Li, D. Lei and J. Lu, *Nano Lett.*, 2022, **22**, 8397-8405.
13. N. Aouina, H. Cachet, C. Debiemme-chouvy and T. T. M. Tran, *Electrochim. Acta*, 2010, **55**, 7341-7345.